Nuclear Physics A559 (1993) 1–41
North-Holland

NUCLEAR PHYSICS A

Strength distributions in neodymium isotopes: a test of collective nuclear models

M. Pignanelli,[a] N. Blasi,[a] J.A. Bordewijk,[b] R. De Leo,[c] M.N. Harakeh,[d] M.A. Hofstee,[b] S. Micheletti,[a] R. Perrino,[e] V.Yu. Ponomarev,[d,f] V.G. Soloviev,[f] A.V. Sushkov[f] and S.Y. van der Werf[b]

[a]*Dipartimento di Fisica dell'Università and Sezione INFN, via Celoria 16, I-20133 Milan, Italy*
[b]*Kernfysisch Versneller Instituut, 9747 AA Groningen, The Netherlands*
[c]*Dipartimento di Fisica dell'Università, I-70100 Bari, Italy and Sezione INFN di Lecce, I-73100, Lecce, Italy*
[d]*Faculteit Natuurkunde en Sterrekunde, Vrije Universiteit, De Boelelaan 1081, 1081 HV Amsterdam, The Netherlands*
[e]*Università di Lecce and Sezione INFN di Lecce, I-73100 Lecce, Italy*
[f]*Laboratory of Theoretical Physics, Joint Institute for Nuclear Research, Dubna, Head Post Office, P.O. Box 79, Moscow, Russian Federation*

Received 15 October 1992

Abstract: Excited states in even Nd isotopes, up to excitation energies of 3–4 MeV, were investigated in proton- and deuteron-scattering experiments performed with high-energy resolution. More than 300 transitions were studied. For several new excited states spin and parity assignments have been suggested. Reduced transition probabilities were extracted for natural-parity states from 0^+ up to 6^+. The experimental strength distributions have been compared with the predictions of the interacting boson model (IBM) and of the quasi-particle-phonon model (QPM). The octupole transition probabilities are well described in both models as produced by the fragmentation of the f-boson or of E3 phonons. IBM-sdf calculations seem to account also for the transitions to the low-lying 1^- states. Quadrupole and hexadecapole distributions are well described in the QPM. The leading configurations are due to 6–8 low-lying one-phonon states. The two- and three-phonon states play an important role especially in ^{146}Nd. The failure of IBM quadrupole and hexadecapole calculations clearly points out the need of introducing additional bosons lying at high excitation energies. QPM evaluations account also for other features of the experimental data, as the E5 and E6 strength distributions and the isovector components. The limits of the two models are discussed.

E NUCLEAR REACTIONS ^{142,144,146,148,150}Nd(p, p'), $E = 30.5$ MeV; ^{144}Nd(p, p'), $E = 51$ MeV; ^{142,144,146,148,150}Nd(d, d'), $E = 50.8$ MeV; measured $\sigma(E_p, \theta)$, $\sigma(E_d, \theta)$. ^{142,144,146,148,150}Nd deduced levels, J, π, $B(\lambda)$. Enriched targets.

1. Introduction

The family of stable even-even neodymium isotopes ($Z = 60$, $N = 82$–90) is characterized by a fast transition from spherical to axially deformed shapes and

Correspondence to: Prof. M. Pignanelli, Dipartimento di Fisica, Universitá degli Studi di Milano, Via Celoria 16, 20133 Milan, Italy.

provides, therefore, a sensitive testing ground for nuclear models as many properties are changing rapidly at the onset of deformation. For this reason, these nuclei have received special attention during the past years. Their low-lying states have been studied by different methods as reported in recent compilations [1]).

Electric multipole transition strengths (Eλ-strengths) are currently used in assessing the validity of the different models. Experimental methods extensively used to determine dipole and quadrupole strengths are based on γ-ray absorption or decay and on Coulomb-excitation measurements. Octupole, hexadecapole and higher multipolarity transitions are better observed in inelastic-scattering experiments. The excitation of several final states in Nd isotopes has been recently observed in high-resolution electron-scattering experiments [2-4]). The charge transition densities deduced from these experiments constitute a powerful and direct test of the nuclear wave functions. The strength of the different multipolarities seems to be, in Nd isotopes as well as in other medium-mass nuclei, strongly fragmented[5,6]). For this reason detailed information on strength distributions, weak components included, is hard to obtain from the analysis of (e, e') spectra, because of the radiative tail background. In contrast hadron-scattering data for transitions leading to excitation energies up to a few MeV, where the experimental spectra appear as ensembles of discrete lines, do not suffer from background originating from physical processes. Presently available data on E3 and E4 strength distributions have, therefore, been obtained mostly from hadron-scattering experiments and, in particular, from (p, p') experiments [5-7]).

The present study is addressed to a better understanding of the level structure of these nuclei through the determination of transition strengths as obtained from proton and deuteron inelastic-scattering experiments. The experimental results are compared with theoretical predictions obtained from two different models: the quasi-particle-phonon model (QPM) [8,9]) and the interacting boson model (IBM) [10]).

2. Experimental method

Differential elastic and inelastic cross sections have been measured for proton and deuteron scattering on ^{142,144,146,148,150}Nd using momentum-analyzed beams from the KVI cyclotron. The incident energies were about 30.5 and 50.8 MeV, respectively, for protons and deuterons. The ^{144}Nd(p, p') reaction has been studied also at 51 MeV. Enriched targets, with thicknesses of the order of 1 mg/cm^2 have been used. Detailed information on the incident energy, on the highest excitation energy measured and on the target isotopic enrichment is given for each nucleus in table 1.

The scattered particles were detected in the focal plane of the QMG/2 spectrograph with an energy resolution of 12–15 keV in (p, p') and of 15–22 keV in (d, d') experiments. The excitation energies were determined through the calibration of the focal plane with known excitation energies. On the average the energy values quoted in the present paper have an uncertainty of less than 2 keV for states below 2.2 MeV

TABLE 1

Nd isotope masses, proton and deuteron incident energies, the highest measured excitation energy, E_{max}, the isotopic enrichment of the targets and (e, e') experiments considered in the analysis

A	E_p (MeV)	E_d (MeV)	E_{max} (MeV)	Enrichment (%)	(e, e') data
142	30.3	50.9	5.560	95.6	ref. [2])
144	30.3; 51.0	51.1	3.658	96.6	ref. [27])
146	30.7	50.7	3.760	97.0	ref. [4])
148	30.5	50.5	3.250	96.3	[a])
150	30.7	50.7	3.350	97.0	ref. [3])

[a]) M.N. Harakeh, private communication.

and a larger uncertainty, up to 4 keV, at higher energies, due to the lack of reference levels.

Cross-section values have been derived from the yield in each energy peak. The accuracy in the cross-section normalization has been estimated to be of the order of 10%. This has been tested comparing the elastic-scattering cross sections for each nucleus and each projectile to optical-model predictions. The relative cross-section values should have a slightly better accuracy for the different projectiles on the same target nucleus and a much better accuracy for transitions to different final states excited in the same reaction. Some weak transitions, leading to states lying in the proximity of other more strongly excited states, were detected only in proton scattering because of the better energy resolution. The weakest transitions detected have differential (p, p') cross sections reaching, at the maximum of the angular distribution, a value of the order of 10–20 μb/sr. These cross sections correspond to values of the coupling amplitudes β_λ, of about 0.008–0.010.

3. Data analysis

3.1. SPIN-PARITY ASSIGNMENTS

Spins and parities (J^π) of the states excited by inelastic scattering can be obtained from the transferred angular momentum λ, deduced from the comparison between experimental and calculated differential cross sections. In the present study coupled-channel (CC) calculations have been carried out in order to discriminate between one- and two-step excitations. The calculations have been performed with the code ECIS [11]), using the optical-model parameters of Becchetti and Greenlees [12]) and Daehnick *et al.* [13]) for proton and deuteron scattering, respectively.

A large part of the J^π assignments has been obtained both from (p, p') and (d, d') angular distributions without uncertainties. For some transitions the assignment was less straightforward. Difficulties were encountered in the case of transitions of weak

intensity and not well resolved from neighbouring and stronger transitions. In some other cases a given transition appeared in the energy spectra as a well-resolved peak with a strong intensity, but the angular distribution did not show any characteristic diffraction pattern and does not indicate, therefore, any definite angular-momentum transfer. This result could be due to the presence of two or more overlapping levels. In such a case the J^π is not given or one or two possible assignments are given between parentheses. Other difficulties, as discussed below, arise from uncertainties in the reaction mechanism and the transition form factors.

The spin and parity assigned to each final state, as well as the coupling amplitudes used in CC calculations, β_λ^{pp} and β_λ^{dd}, are given in tables 2-6.

3.2. MULTIPOLE MATRIX ELEMENTS

The transition matrix elements can be derived from the coupling amplitudes:

$$\tilde{M}_{xx}(E\lambda) = Z\beta_\lambda^{xx} \frac{\int V_{tr}^{(\lambda)}(r) r^{\lambda+2}\, dr}{\int V(r)\, dr}, \tag{1}$$

where Z is the atomic number and $V(r)$ and $V_{tr}^{(\lambda)}(r)$ are the real parts of the g.s. optical-model potential and of the transition potential, respectively. The reduced transition probabilities are obtained from the matrix elements: $\tilde{B}_{xx}(E\lambda, J_i \to J_f) = |\tilde{M}_{xx}(E\lambda)|^2/(2J_i+1)$. Expression (1), which holds for $\lambda \geqslant 2$, gives the transition matrix elements in terms of transition potentials. According to the Satchler theorem [14]), these matrix elements should be equal to the matrix elements of the transition mass-densities. As discussed by Bernstein *et al.* [15]), eq. (1) is a "modified" form of the matrix elements, since their values are obtained using the atomic number Z instead of the mass number A. In the following the "modified" and the "non-modified" transition matrix elements are written as $\tilde{M}_{xx}(E\lambda)$ and $M_{xx}(E\lambda)$, respectively. The expressions that connect "modified" and "non-modified" quantities are given in refs. [5,6]). The modified values make easier the comparison between data obtained from different measurements since the transition probabilities from hadron scattering become equal to the electromagnetic probabilities in absence of isovector contributions. The transition probabilities quoted in the present paper are the "modified" values as currently used in the literature. The different definitions of the matrix elements must be taken properly into account when transition probabilities from different experiments are compared with model predictions.

Dropping the indication of the multipolarity, we indicate hereafter with M_{ee}, $\tilde{M}_{pp}$ and $\tilde{M}_{dd}$ the transition matrix elements deduced from (e, e'), (p, p') and (d, d') experiments, respectively. These quantities can be expressed in terms of the proton and neutron matrix elements and vice versa:

$$M_{ee} = M_p = \frac{A}{Z}(3\tilde{M}_{dd} - 2\tilde{M}_{pp}), \tag{2}$$

TABLE 2

Spectroscopic information deduced for ^{142}Nd from inelastic proton and deuteron scattering. Level energy, E_x, spin-parity J^π, coupling parameters β_λ^{pp} and β_λ^{dd}, and isoscalar transition probability $\tilde{B}_S(E\lambda)$ (and error) are given for each level

E_x (MeV)	J_f^π	β_λ^{pp}	β_λ^{dd}	$\tilde{B}_S(E\lambda)$ (W.u.)	E_x (MeV)	J_f^π	β_λ^{pp}	β_λ^{dd}	$\tilde{B}_S(E\lambda)$ (W.u.)
1.576	2^+	0.0810	0.0900	14.0 (0.71)	4.180	(4^+)	0.0110		0.36 (0.03)
2.084	3^-	0.1270	0.1180	34.1 (1.4)	4.201	2^+	0.0164	0.0129	0.29 (0.04)
2.101	4^+	0.0627	0.0640	15.9 (0.85)	4.272	5^-	0.0160		1.29 (0.14)
2.209	(6^+)	0.0260	0.0231	6.97 (0.50)	4.285	3^-	0.0137	0.0124	0.38 (0.03)
2.217	0^+	0.0039	0.0046	0.22 (0.05)	4.298	(5^-)	0.0140		0.99 (0.10)
2.244	1^-	0.0017	0.0024	0.10 (0.03)	4.326	6^+	0.0256	0.0140	2.56 (0.35)
2.384	2^+	0.0238	0.0239	0.99 (0.07)	4.346	6^+	0.0126	0.0077	0.77 (0.14)
2.438	4^+	0.0194	0.0180	1.26 (0.06)	4.383	1^-	0.0015	0.0022	0.08 (0.02)
2.515	(1^-)	0.0025	0.0017	0.07 (0.02)	4.426	(3^-)	0.0200	0.0126	0.39 (0.05)
2.549	(1^-)	0.0026	0.0019	0.11 (0.02)	4.456	3^-	0.0102	0.0110	0.29 (0.03)
2.583	2^+	0.0180	0.0170	0.50 (0.04)	4.464				
2.736	(4^+)	0.0190	0.0145	0.82 (0.11)	4.481	(4^+)	0.0126	0.0131	0.67 (0.06)
2.776	1^-	0.0017	0.0019	0.09 (0.02)	4.497	2^+	0.0111	0.0090	0.14 (0.02)
2.846	2^+	0.0387	0.0387	2.58 (0.14)	4.515	3^-	0.0120		0.29 (0.04)
2.885	(6^+)	0.0118	0.0077	0.77 (0.08)	4.530				
2.975	5^-	0.0560	0.0410	11.4 (0.71)	4.550				
3.008	(3^-)	0.0108	0.0108	0.29 (0.02)	4.567	2^+	0.0117	0.0105	0.19 (0.03)
3.045	2^+	0.0173	0.0173	0.52 (0.04)	4.581	2^+	0.0100		0.14 (0.02)
3.080	4^+	0.0304	0.0281	3.07 (0.15)	4.626	3^-	0.0175	0.0105	0.27 (0.03)
3.126	2^+	0.0105	0.0118	0.24 (0.02)	4.638	(2^+)	0.0077		0.09 (0.02)
3.241	7^-	0.0300	0.0173	12.3 (1.3)	4.662	5^-	0.0164		1.35 (0.14)
3.295	5^-	0.0140	0.0110	0.82 (0.08)	4.688	5^-	0.0173		1.50 (0.07)
3.315	4^+	0.0391	0.0354	4.87 (0.24)	4.707	3^-	0.0158	0.0130	0.41 (0.07)
3.408	6^+	0.0310	0.0256	8.57 (0.71)	4.725				
3.420	1^-	0.0046	0.0040	0.42 (0.09)	4.744	(0^+)	0.0031		0.09 (0.02)
3.499	(7^-)	0.0200	0.0110	5.26 (0.71)	4.752	6^+	0.0164		2.45 (0.30)
3.541	(7^-)	0.0100	0.0092	2.06 (0.36)	4.798	3^-	0.0216	0.0171	0.72 (0.06)
3.576	3^-	0.0364	0.0260	1.66 (0.17)	4.838	(3^-)	0.0200	0.0142	0.49 (0.08)
3.594	5^-	0.0160	0.0148	1.49 (0.11)	4.847				
3.632	6^+	0.0122		1.36 (0.16)	4.862				
3.675	6^+	0.0084		0.64 (0.13)	4.892	3^-	0.0102	0.0130	0.41 (0.04)
3.707	(3^-)	0.0255	0.0173	0.73 (0.07)	4.908	$(3^-, 4^+)$			
3.762	(0^+)	0.0033	0.0031	0.10 (0.02)	4.971				
3.783	3^-	0.0235	0.0180	0.79 (0.07)	4.993	4^+	0.0218	0.0167	1.08 (0.11)
3.806	(4^+)	0.0122	0.0112	0.49 (0.07)	5.040	3^-	0.0210	0.0130	0.41 (0.06)
3.834	(0^+)	0.0030	0.0020	0.04 (0.02)	5.054				
3.871	$(4^-, 5^-)$				5.089	3^-	0.0316	0.0250	1.53 (0.14)
3.897	0^+	0.0021		0.06 (0.01)	5.102	$(0^+, 1^-)$			
3.908	$(2^-, 5^-)$				5.130	(3^-)	0.0243	0.0170	0.71 (0.06)
3.923	(1^-)	0.0036	0.0033	0.26 (0.05)	5.145	2^+	0.0091		0.12 (0.02)
3.935					5.162	(1^-)	0.0023	0.0026	0.09 (0.02)
3.983	6^+	0.0187		3.19 (0.04)	5.172	(3^-)	0.0104		0.21 (0.03)
4.004	4^+	0.0150	0.0122	0.52 (0.06)	5.193				
4.076					5.228	4^+	0.0128	0.0090	0.31 (0.04)
4.104	4^+	0.0169	0.0117	0.53 (0.04)	5.252	2^+	0.0078	0.0084	0.12 (0.02)
4.127					5.266	4^+	0.0119		0.43 (0.07)
4.153	(5^-)	0.0126		0.80 (0.06)	5.277	2^+	0.0100	0.0083	0.12 (0.02)

TABLE 2—continued

E_x (MeV)	J_f^π	β_λ^{pp}	β_λ^{dd}	$\tilde{B}_S(E\lambda)$ (W.u.)	E_x (MeV)	J_f^π	β_λ^{pp}	β_λ^{dd}	$\tilde{B}_S(E\lambda)$ (W.u.)
5.322					5.471				
5.332	3^-	0.0128		0.32 (0.04)	5.496				
5.355	$(2^+, 3^-)$				5.511	3^-	0.0172	0.0171	0.72 (0.06)
5.377	0^+	0.0030	0.0030	0.09 (0.02)	5.525	3^-	0.0222	0.0175	0.75 (0.06)
5.412	$(0^+, 1^-)$				5.552				
5.433									

The $\tilde{B}_S(E\lambda)$ values are given in Weisskopf single-particle unit (W.u.):
$B_{s.p.u.}(E0) = A^{2/3}\ (e^2 \cdot \mathrm{fm}^4)$; $B_{s.p.u.}(E1) = (3/64\pi)(1.2A^{1/3})^6\ (e^2 \cdot \mathrm{fm}^6)$;
$B_{s.p.u.}(E\lambda) = [(2\lambda+1)/4\pi]\ [3/(\lambda+3)]^2\ (1.2A^{1/3})^{2\lambda}\ (e^2 \cdot \mathrm{fm}^{2\lambda})$, with λ is ≥ 2.
The W.u. for E0 and E1 are defined in refs. [16,17]), respectively.

TABLE 3

Same as table 2 for ^{144}Nd

E_x (MeV)	J_f^π	β_λ^{pp}	β_λ^{dd}	$\tilde{B}_S(E\lambda)$ (W.u.)	E_x (MeV)	J_f^π	β_λ^{pp}	β_λ^{dd}	$\tilde{B}_S(E\lambda)$ (W.u.)
0.696	2^+	0.1200	0.1180	24.0 (1.2)	2.717	(1^-)	0.0032	0.0030	0.22 (0.04)
1.314	4^+	0.0600	0.0530	10.8 (1.0)	2.779	3^-	0.0560	0.0547	7.29 (0.70)
	$2_1^+ \rightarrow 4^+$	0.1450	0.1230		2.833	3^-	0.0231	0.0218	1.16 (0.12)
1.510	3^-	0.1255	0.1180	33.9 (1.7)	2.898	2^+	0.0131	0.0105	0.19 (0.02)
1.561	2^+	0.0130	0.0140	0.34 (0.06)	2.969	3^-	0.0264	0.0200	0.97 (0.10)
	$2_1^+ \rightarrow 2^+$	0.1600	0.1900		2.987	4^+	0.0280	0.0250	2.41 (0.22)
1.791	6^+	0.0200	0.0190	3.78 (0.35)	3.026	5^-	0.0220	0.0200	2.68 (0.24)
2.073	2^+	0.0310	0.0330	1.87 (0.13)	3.049	5^-	0.0490	0.0440	13.0 (1.4)
	$2_1^+ \rightarrow 2^+$	−0.0800	−0.0800		3.097	$(0^+, 1^-)$			
2.093	5^-	0.0548	0.0400	10.7 (1.0)	3.130	1^-	0.0029	0.0028	0.19 (0.04)
2.109	4^+	0.0560	0.0520	10.4 (0.83)	3.180	(6^+)	0.0260	0.0170	3.01 (0.42)
2.185	(1^-)	0.0066	0.0066	0.98 (0.21)	3.214	3^-	0.0098	0.0105	0.27 (0.03)
2.217	(6^+)	0.0310		7.78 (1.4)	3.240	(3^-)	0.0080	0.0082	0.16 (0.03)
2.295	4^+	0.0097	0.0101	0.39 (0.04)	3.289	(3^-)	0.0170	0.0140	0.48 (0.07)
2.327	(0^+)	0.0028	0.0030	0.10 (0.02)	3.340	4^+	0.0152	0.0158	0.96 (0.15)
2.367	2^+	0.0238	0.0241	1.00 (0.06)	3.382	(4^+)	0.0148	0.0148	0.84 (0.10)
2.451	4^+	0.0232	0.0230	2.04 (0.19)	3.401	5^-	0.0190		1.77 (0.35)
2.527	2^+	0.0303	0.0300	1.55 (0.14)	3.461	4^+	0.0128	0.0128	0.63 (0.11)
2.590	(1^-)	0.0038		0.29 (0.06)	3.493	5^-	0.0224	0.0182	2.22 (0.19)
2.606					3.522	2^+	0.0170		0.41 (0.08)
2.675	(0^+)	0.0026	0.0024	0.06 (0.02)	3.555	2^+	0.0134		0.25 (0.04)
2.694	2^+	0.0105	0.0098	0.17 (0.02)	3.658	3^-	0.0164		0.56 (0.08)

TABLE 4
Same as table 2 for ^{140}Nd

E_x (MeV)	J_f^π	β_λ^{pp}	β_λ^{dd}	$\tilde{B}_S(E\lambda)$ (W.u.)	E_x (MeV)	J_f^π	β_λ^{pp}	β_λ^{dd}	$\tilde{B}_S(E\lambda)$ (W.u.)
0.454	2^+	0.1610	0.1580	42.9 (3.4)	2.705	(6^+)	0.0170	0.0150	2.83 (0.34)
0.918	0^+		0.0034	0.12 (0.02)	2.747	5^-	0.0270	0.0228	3.45 (0.30)
1.043	4^+	0.0450	0.0400	6.11 (0.27)	2.807				
	$2_1^+ \to 4^+$	0.1890	0.1680		2.821	3^-	0.0138	0.0134	0.43 (0.07)
1.190	3^-	0.1438	0.1310	41.6 (2.0)	2.847	3^-	0.0282	0.0260	1.64 (0.15)
1.376	1^-		0.0085	1.76 (0.34)	2.874	(2^+)	0.0130	0.0140	0.34 (0.03)
1.471	2^+	0.0360	0.0360	2.22 (0.12)	2.887				
	$2_1^+ \to 2^+$	0.1080	0.1080		2.916	5^-	0.0240	0.0212	2.98 (0.30)
1.517	5^-	0.0570	0.0490	15.9 (1.0)	2.932	4^+	0.0243	0.0223	1.90 (0.22)
	$2_1^+ \to 5^-$	−0.134	−0.110		2.973	2^+	0.0141	0.0141	0.34 (0.03)
	$3_1^- \to 5^-$	−0.141	−0.117		3.005	5^-	0.0235	0.0189	2.37 (0.24)
1.572	(0^+)	0.0030	0.0032	0.11 (0.02)	3.018	3	0.0125		0.28 (0.05)
1.695	(0^+)		0.0028	0.08 (0.02)	3.095	4^+	0.0158		0.72 (0.15)
1.744	4^+	0.0678	0.0606	14.0 (0.68)	3.103	2^+	0.0077	0.0089	0.14 (0.02)
1.780	6^+	0.0208		2.99 (0.72)	3.150	6^+	0.0148		1.51 (0.22)
1.787	2^+	0.0173	0.0168	0.48 (0.09)	3.162	4^+	0.0158	0.0141	0.76 (0.08)
1.917	(4^+)	0.0166	0.0144	0.79 (0.16)	3.209	4^+	0.0141	0.0141	0.76 (0.09)
1.976	(2^+)	0.0210	0.0190	0.62 (0.08)	3.231	(4^-)			
1.988	4^+	0.0418	0.0415	6.58 (0.34)	3.249	3^-	0.0130	0.0106	0.27 (0.02)
2.027	1^-	0.0031		0.20 (0.04)	3.273	(6^+)	0.0110		0.84 (0.14)
2.069	5^-	0.0186		1.66 (0.24)	3.285	2^+	0.0077		0.08 (0.02)
	$2_1^- \to 5^-$	0.0610			3.311	4^+	0.0195	0.0158	0.96 (0.14)
	$3_1^- \to 5^-$	0.0087			3.355	3^-	0.0160	0.0148	0.53 (0.07)
2.090	(0^+)	0.0045	0.0050	0.26 (0.05)	3.421	(0^+)	0.0030	0.0028	0.08 (0.02)
2.198	2^+	0.0114	0.0105	0.19 (0.02)	3.435	5^-	0.0135		0.87 (0.10)
2.225	1^-	0.0031	0.0035	0.25 (0.04)	3.454	4^+	0.0122		0.43 (0.04)
2.269	1^-	0.0031	0.0035	0.25 (0.04)	3.472	4^+	0.0177	0.0180	1.24 (0.11)
2.335	3^-	0.0560	0.0520	6.55 (0.41)	3.485	2^+	0.0120		0.20 (0.02)
2.453	2^+	0.0100	0.0100	0.17 (0.03)	3.503	5^-	0.0145	0.0130	1.12 (0.11)
2.478	(2^+)	0.0119	0.0111	0.21 (0.03)	3.539	2^+	0.0089		0.11 (0.02)
2.525	3^-	0.0410	0.0380	3.50 (0.20)	3.567	5^-	0.0140		0.94 (0.14)
2.552	4^+	0.0200	0.0173	1.14 (0.08)	3.585	2^+	0.0077		0.08 (0.02)
2.570	5^-	0.0328	0.0280	5.20 (1.0)	3.616	5^-	0.0147	0.0170	1.92 (0.15)
2.622	4^+	0.0189	0.0177	1.20 (0.11)	3.624	2^+	0.0110		0.17 (0.03)
2.665	2^+	0.0148	0.0158	0.43 (0.05)	3.676	5^-		0.0178	2.10 (0.34)
2.687	(3^-)	0.0118	0.0100	0.24 (0.03)	3.755	(4^+)		0.0137	0.72 (0.15)

$$\tilde{M}_{pp} = \frac{Z}{A}\left(\tfrac{3}{2}M_n + \tfrac{1}{2}M_p\right), \tag{3}$$

$$\tilde{M}_{dd} = \frac{Z}{A}\left(M_n + M_p\right). \tag{4}$$

The second relation (2) and eq. (3) are obtained taking into account the fact that at low incident energies the proton–neutron interaction is three times larger than

TABLE 5

Same as table 2 for ^{148}Nd

E_x (MeV)	J_f^π	β_λ^{pp}	β_λ^{dd}	$\tilde{B}_S(E\lambda)$ (W.u.)	E_x (MeV)	J_f^π	β_λ^{pp}	β_λ^{dd}	$\tilde{B}_S(E\lambda)$ (W.u.)
0.303	2^+	0.1980	0.1970	66.5 (5.3)	2.197	5^-	0.0333	0.0300	5.90 (0.66)
0.752	4^+	0.0539	0.0490	8.21 (0.85)	2.257	(2^+)	0.0171	0.0163	0.46 (0.05)
	$2_1^+ \to 4^+$	0.2300	0.2100		2.286	(3^-)	0.0121	0.0101	0.25 (0.03)
0.920	0^+	0.0036	0.0044	0.21 (0.04)	2.341	3^-	0.0187	0.0158	0.60 (0.03)
0.998	3^-	0.1420	0.1260	38.3 (1.8)	2.388	4^+	0.0242	0.0157	0.84 (0.10)
1.022	1^-	0.0110		2.39 (0.33)	2.429	2^+	0.0163	0.0171	0.50 (0.05)
1.171	2^+	0.0209	0.0193	0.64 (0.05)	2.484	3^-	0.0125	0.0115	0.32 (0.02)
	$2_1^+ \to 2^+$	−0.104	−0.094		2.544	(1^-)	0.0025	0.0026	0.14 (0.04)
1.244	2^+	0.0460	0.0460	3.63 (0.39)	2.590	4^+	0.0280	0.0221	1.67 (0.16)
	$2_1^+ \to 2^+$	0.0600	0.0600		2.642	4^+	0.0110		0.35 (0.04)
1.400	$(0^+, 1^-)$				2.682	0^+	0.0039	0.0039	0.16 (0.03)
1.432	$(0^+, 1^-)$				2.709	4^+	0.0187	0.0179	1.10 (0.06)
1.475	(1^-)	0.0020		0.08 (0.02)	2.770	4^+	0.0190	0.0174	1.03 (0.08)
1.577	2^+	0.0113	0.0111	0.21 (0.02)	2.807	3^-	0.0123	0.0129	0.40 (0.05)
1.602	4^+	0.0144	0.0128	0.56 (0.06)	2.871	(3^-)	0.0153	0.0137	0.45 (0.06)
1.654	(3^-)	0.0170	0.0167	0.67 (0.13)	2.913	4^+	0.0216	0.0189	1.22 (0.10)
1.685	4^+	0.0630	0.0552	10.4 (0.85)	2.961	4^+	0.0159	0.0137	0.64 (0.06)
1.725	3^-	0.0696	0.0597	8.59 (0.45)	3.022	4^+	0.0200	0.0139	0.66 (0.07)
1.778	(3^-)	0.0089	0.0083	0.19 (0.02)	3.068	(3^-)	0.0089		0.16 (0.02)
1.837	(1^-)	0.0036	0.0036	0.28 (0.06)	3.096	(1^-)	0.0019		0.07 (0.02)
1.887	4^+	0.0310	0.0296	3.00 (0.28)	3.142	4^+	0.0241	0.0171	1.00 (0.15)
2.034	3^-	0.0348	0.0323	2.51 (0.20)	3.191	4^+	0.0163	0.0126	0.54 (0.07)
2.098	4^+	0.0414	0.0349	4.17 (0.26)	3.241	4^+	0.0214	0.0150	0.77 (0.09)
2.145	4^+	0.0122		0.43 (0.05)					

the proton-proton interaction. Finally, following ref. [15]), we can obtain the non-modified and the modified isoscalar and isovector matrix elements from the expressions:

$$M_S = \tfrac{1}{2}(M_n + M_p) = M_{dd} = \frac{A}{Z}\tilde{M}_{dd}\,, \tag{5a}$$

$$\tilde{M}_S = \frac{Z}{A}(M_n + M_p) = \tilde{M}_{dd}\,, \tag{5b}$$

$$M_V = \tfrac{1}{2}(M_n - M_p) = 2(M_{pp} - M_{dd}) = 2\frac{A}{Z}(\tilde{M}_{pp} - \tilde{M}_{dd})\,, \tag{6a}$$

$$\tilde{M}_V = \frac{Z}{A}(M_n - M_p) = 2(\tilde{M}_{pp} - \tilde{M}_{dd})\,. \tag{6b}$$

In comparing experimental and theoretical values one should remember that the IBM-1 model does not distinguish between proton and neutron degrees of freedom and consequently it cannot be used to calculate M_V, M_p and M_n but only the $\tilde{M}_S$ values. These latter matrix elements can be compared directly with the experimental

TABLE 6

Same as table 2 for ^{150}Nd

E_x (MeV)	J_f^π	β_λ^{pp}	β_λ^{dd}	$\tilde{B}_S(E\lambda)$ (W.u.)	E_x (MeV)	J_f^π	β_λ^{pp}	β_λ^{dd}	$\tilde{B}_S(E\lambda)$ (W.u.)
0.130	2^+	0.2450	0.2300	115.0 (8.6)	2.206	4^+	0.0187	0.0148	0.82 (0.13)
0.381	4^+	0.0500	0.0480	34.2 (2.6)	2.223	2^+	0.0180	0.0155	0.41 (0.04)
0.675	0^+		0.0063	0.43 (0.06)	2.242	2^+	0.0152	0.0158	0.43 (0.03)
0.720	6^+	0.0020	0.0025	11.3 (1.3)	2.271	3^-	0.0190	0.0170	0.69 (0.08)
0.851	1^-	0.0082	0.0100	1.93 (0.04)	2.328	3^-	0.0210	0.0170	0.69 (0.13)
0.934	3^-	0.1060	0.0950	21.6 (1.1)	2.384	2^+	0.0190	0.0148	0.37 (0.03)
1.062	2^+	0.0500	0.0460	3.62 (0.26)	2.412	3^-	0.0270	0.0250	1.50 (0.22)
1.129	(5^-)		0.0320	6.62 (0.96)	2.441	4^+	0.0224	0.0170	1.09 (0.10)
1.285	$(0^+, 1^-)$				2.475	4^+	0.0316	0.0245	2.26 (0.22)
1.318	(1^-)	0.0029	0.0039	0.26 (0.05)	2.498	$(1^-, 4^+)$			
1.354	4^+	0.0245	0.0223	1.87 (0.16)	2.528	4^+	0.0210		1.24 (0.20)
1.408	(2^+)	0.0084	0.0088	0.13 (0.02)	2.563	4^+	0.0210		1.24 (0.18)
1.435	4^+	0.0247	0.0200	1.50 (0.19)	2.596	5^-	0.0240		2.65 (0.35)
1.485	3^-	0.0490	0.0450	4.86 (0.49)	2.638	4^+	0.0235	0.0182	1.25 (0.08)
1.518	3^-	0.0260	0.0200	0.96 (0.10)	2.652	4^+	0.0158		0.70 (0.17)
1.546	3^-	0.0180	0.0190	0.87 (0.09)	2.681	4^+	0.0200		1.12 (0.12)
1.582	3^-	0.0394	0.0367	3.23 (0.26)	2.707	4^+	0.0170		0.81 (0.09)
1.604					2.737	4^+	0.0170	0.0150	0.85 (0.06)
1.648	4^+	0.0358	0.0245	2.26 (0.10)	2.755	4^+	0.0224	0.0197	1.46 (0.13)
1.687	3^-	0.0150	0.0120	0.35 (0.05)	2.789	4^+	0.0212	0.0138	0.72 (0.06)
1.740	0^+	0.0040	0.0041	0.18 (0.03)	2.818	3^-	0.0150		0.42 (0.04)
1.754	(4^+)	0.0130		0.47 (0.04)	2.836	3^-	0.0223	0.0200	0.96 (0.10)
1.782	4^+	0.0130	0.0134	0.67 (0.04)	2.880	3^-	0.0250		1.16 (0.12)
1.802	(5^-)	0.0160		1.18 (0.13)	2.895	4^+	0.0224	0.0224	1.89 (0.13)
1.830	(5^-)	0.0140		0.90 (0.12)	2.925	4^+	0.0190		1.01 (0.20)
1.866	3^-	0.0330	0.0283	1.92 (0.10)	2.961	2^+	0.0155		0.33 (0.04)
1.885	4^+	0.0182	0.0140	0.74 (0.11)	2.993	$(1^-, 4^+)$			
1.906	4^+	0.0245	0.0194	1.41 (0.11)	3.039	4^+	0.0200	0.0170	1.09 (0.13)
1.921	4^+	0.0170	0.0190	1.36 (0.11)	3.069	3^-	0.0190	0.0170	0.69 (0.08)
1.988	3^-	0.0160	0.0160	0.61 (0.09)	3.085	4^+	0.0164		1.16 (0.13)
2.008	2^+	0.0150	0.0150	0.38 (0.03)	3.112	2^+	0.0148	0.0148	0.37 (0.03)
2.033	4^+	0.0200	0.0187	1.31 (0.13)	3.157	(2^+)	0.0134		0.25 (0.03)
2.055	2^+	0.0220	0.0180	0.55 (0.04)	3.180	(2^+)	0.0141	0.0141	0.34 (0.03)
2.077	3^-	0.0250	0.0220	1.16 (0.12)	3.221	(2^+)	0.0180	0.0160	0.44 (0.08)
2.090	3^-	0.0230		0.99 (0.24)	3.252	4^+	0.0200		1.12 (0.13)
2.109	3^-	0.0350	0.0250	1.50 (0.15)	3.301	4^+	0.0130		0.47 (0.11)
2.129	4^+	0.0253	0.0219	1.80 (0.13)	3.315	3^-	0.0180		0.60 (0.08)
2.174	4^+	0.0187	0.0158	0.94 (0.09)	3.340	4^+	0.0221		1.37 (0.14)
2.194	2^+	0.0158		0.35 (0.04)					

$\tilde{M}_{dd}$ values. QPM and IBM-2 calculations allow the evaluation of M_p and M_n and these matrix elements can be compared with the experimental results using eqs. (5) and (6).

As shown below, the present study provides rather precise information on the isoscalar mass transition probabilities and a less accurate, but still significant

evaluation of the isovector components. The isoscalar mass transition probabilities, $\tilde{B}_S(E\lambda)$, have been obtained from (d, d') cross sections. Their values are given, in Weisskopf single-particle units, in columns 5 and 10 of tables 2-6. In absence of (d, d') data the $\tilde{B}_S(E\lambda)$ values have been obtained from the relation: $\tilde{M}_S(E\lambda) = \tilde{M}_{dd} \sim \tilde{M}_{pp}/[1+(N-Z)/2A]$. This expression can be deduced, assuming, as in a simple one-fluid collective model, that $M_p/M_n = Z/N$. As shown below (see also fig. 2), this expression is in good agreement with the average trend of the experimental results. The errors quoted for the $\tilde{B}_S(E\lambda)$ values are only those due to the uncertainty in the normalization of the calculated to the experimental cross sections. Other sources of errors, discussed in the next section, are difficult to estimate and are not included.

3.3. ACCURACY OF CC CALCULATIONS

Possible sources of errors in extracting the transition probabilities are: (i) uncertainties in the absolute normalization of the experimental cross sections; (ii) imprecisions in the relative normalization of the calculated to the experimental differential cross sections and (iii) uncertainties in model analysis. The latter concern mainly the assumptions on the transition form factors and on the role played by two-step processes.

The uncertainties in the absolute cross sections give a negligible contribution to the uncertainty in $\tilde{M}_{xx}(E\lambda)$ values. In fact the coupling parameters β_λ^{xx} are determined essentially by the relative value of the inelastic to the elastic cross sections (i.e. by the fraction of the flux drawn from the elastic into the inelastic channel). Their values are therefore not affected by relatively small changes in absolute cross section values.

Uncertainties in the transition form factors can lead to inaccurate evaluations of the transition probabilities, because the ratio $\sigma(x, x')/\tilde{B}_{xx}(E\lambda)$ is affected by the radial dependence of the transition form factor. In the case of transitions with $\lambda \geq 2$, we have assumed a standard collective form factor given by a first derivative of the ground state (g.s.) potential. Such an assumption, when generalized to all transitions, is crude but not unjustified. The microscopic models produce transition densities with a large variety of radial shapes. However, if a realistic nucleon-nucleon interaction is folded into these densities, one usually obtains surface-peaked transition potentials, which are nearly equivalent to a first derivative of the g.s. potential. As examples we consider here some potentials obtained by folding the Jeukenne-Lejeunne-Mahaux density-dependent effective interaction [18]) into transition densities evaluated in the framework of QPM. As shown in refs. [2-4]) this model gives a successful description to the transition charge densities obtained from Nd(e, e') experiments. We can, therefore, assume with a high degree of confidence, that QPM evaluations well describe also the neutron transition densities. As shown in fig. 1, in the case of five low-lying 2^+ states in ^{144}Nd, the different transition

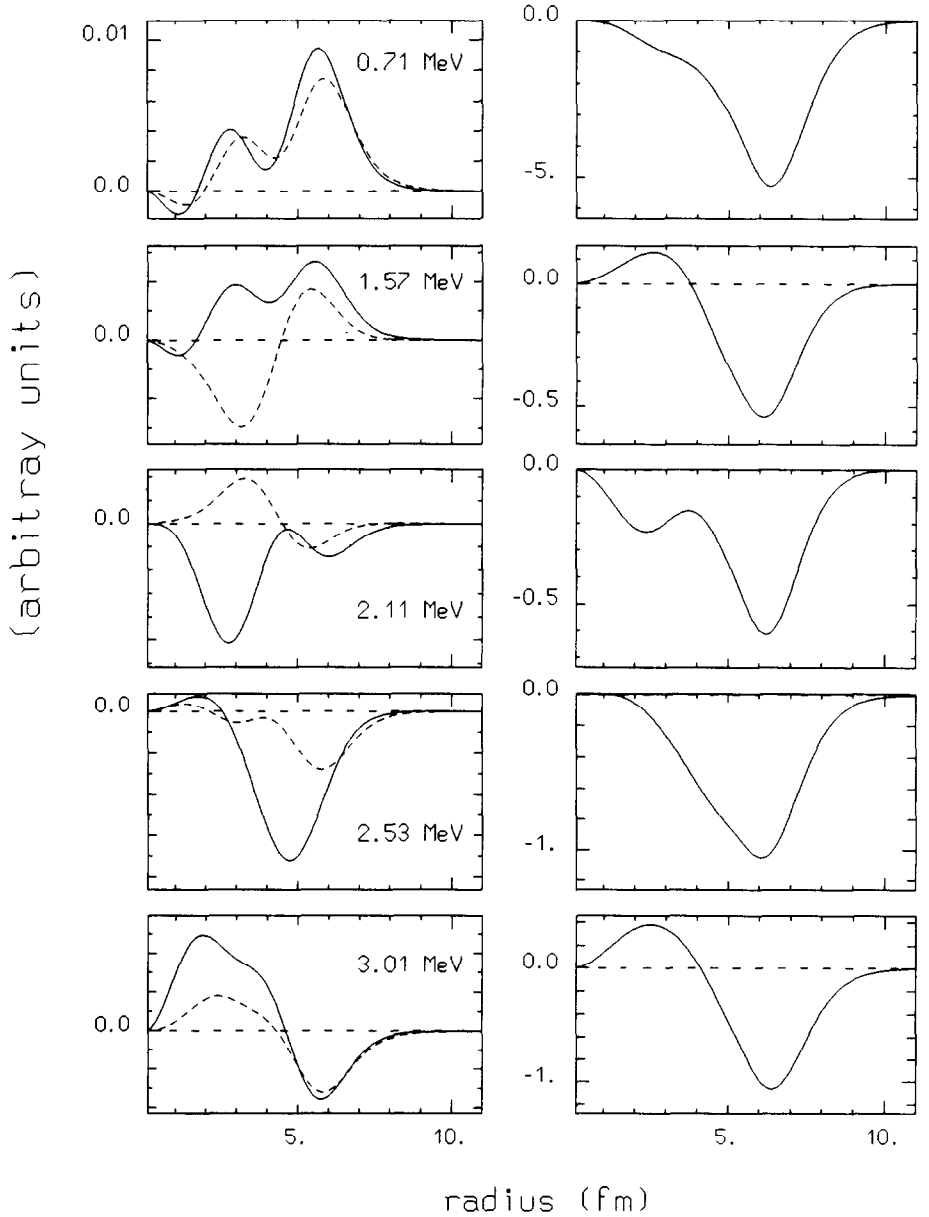

Fig. 1. Transitions to 2^+ states in ^{144}Nd. Left part: proton (full curves) and neutron (dashed curves) transition densities obtained from QPM calculations. Right part: (p, p') real part of the transition potentials obtained by a folding-model procedure.

densities display different radial distributions, often with a complex structure (left part of the figure). However, the transition potentials (right part) obtained from the same transition densities can be nearly always approximated by a first derivative of a Woods-Saxon potential. This result is due to several reasons: (i) in some cases the proton and neutron contributions from the interior of the nucleus cancel each other (levels at 1.57 and 2.11 MeV); (ii) the density dependence of the effective interaction reduces the inner part of the transition potential and leads, therefore, to a surface-peaked potential; (iii) residual inner tails or bumps in the transition potentials are usually much smaller than the peak at the nuclear surface and give, therefore, small contributions to the resulting cross section, also because the sensitivity of the projectile to the interior of the nucleus is very small (deuterons) or reduced (protons). A first derivative shape of the transition form factor seems therefore to be a realistic assumption also in the framework of the QPM.

Finally we have estimated the possible two-step contributions and their effects on the evaluation of transition strengths. In the excitation of vibrational or rotational nuclei, two-step processes can be particularly significant since they are connected to the structure of the target nucleus: the presence of two-phonon states or of roto-vibrations. The latter configurations could play a role in the case of ^{150}Nd, while multi-phonon states could play a role for the other Nd isotopes.

Large two-step contributions to inelastic cross sections arise only from the coupling of the final state with a strong intermediate channel as the 2_1^+ or/and 3_1^- channels. Evidence of two-step processes has been found in the transitions to states belonging to the g.s. rotational band in ^{150}Nd and to a limited number of transitions in ^{144,146,148}Nd. The two-step contributions in these latter nuclei should be connected mainly to two-phonon components in the wave function of the final state: E2-E2 two-phonon components in 0^+, 2^+ and 4^+ states and E2-E3 two-phonon components in 1^-, 3^- and 5^- states. In CC calculations the intensity of the two-step contributions (and therefore the two-phonon strength found in a transition) is determined by the coupling of the final state to the intermediate state. The procedure used to determine these contributions has been extensively described in two recent papers in the case of negative-parity states [5]), and of positive-parity states [6]) (E2-E3 and E2-E2 excitations, respectively). The explicit consideration of two-step contributions leads to a better accuracy in the evaluation of the strengths of the direct transitions. The estimate of the couplings between excited states in this procedure is less accurate. Within the limits of this lower accuracy it might be observed that the β_3 and β_2 values given in tables 3 to 5 for the second step generally do not exhaust the full strength predicted by the vibrational model [19]), thus suggesting a fragmentation of the two-phonon strength. A similar result was found for the E2-E3 strength in the excitation of the 1^-, 3^- and 5^- states in Mo, Pd and Cd isotopes [5]). In contrast, in these latter nuclei the full E2-E2 two-phonon strength was found in the 4_1^+ and 2_2^+ states as well as the full E2-E3 strength in the 2_1^- and 4_1^- states. This last result is particularly significant because the unnatural-parity states are not coupled directly

to the g.s. by Eλ operators and, therefore, the only possible mechanism for their excitation is a multi-step mechanism. In such a case the comparison between experimental and calculated cross sections gives the two-phonon strength without ambiguities and with a good accuracy. In the present experiment we do not find any clear indication for the excitation of unnatural-parity states. This result and the fact that the E2–E2 two-phonon strength seems to be not exhausted in the transitions to the 2_2^+ and 4_1^+ states indicate that the fragmentation of the two-phonon strengths in Nd isotopes is larger than that found in Mo, Pd and Cd isotopes. A fragmentation of the two-phonon components is also predicted by the QPM.

3.4. MONOPOLE AND DIPOLE TRANSITIONS

The spin-parity assignment and the evaluation of transition matrix elements are particularly difficult in the case of monopole and dipole transitions. The main maximum in $\lambda = 0$ and $\lambda = 1$ angular distributions is located at small scattering angles, out of the angular range here explored. Moreover, the transition form factors differ from those for $\lambda \geq 2$ and are less known than for other multipolarities. The conservation of particle number and the translational invariance imply that E0 and E1 transition densities must satisfy the following rules, respectively:

$$\int \rho_{\mathrm{tr}}^{(0)}(r) r^2 \, \mathrm{d}r = 0, \qquad \int \rho_{\mathrm{tr}}^{(1)}(r) r^3 \, \mathrm{d}r = 0 . \tag{7}$$

These rules imply that $\rho_{\mathrm{tr}}^{(0)}(r)$ and $\rho_{\mathrm{tr}}^{(1)}(r)$ must have at least one node near the nuclear surface and the most prominent maximum inside the nucleus. This behaviour of the form factors has been also evidenced in charge transition densities obtained from (e, e′) experiments: 0^+ state at 2.976 MeV in ^{142}Nd [ref. [2])], 1^- states at 1.379 MeV in ^{146}Nd [ref. [4])], at 1.022 MeV in ^{148}Nd and at 0.850 MeV in ^{150}Nd [ref. [3])]. When these transition densities are folded with an effective density-dependent interaction, the resulting transition potential is generally quite similar to a second derivative of the g.s. potential. An example of these folding-model calculations is given in fig. 4 of ref. [5]). We have assumed, therefore, a second-derivative form factor.

The structure of the low-lying 0^+ and 1^- states enhances the two-step processes via the 2_1^+ and 3_1^- states. In fact the wave functions of these states have large two-phonon components. These give rise to contributions to the inelastic cross sections through a direct second-order coupling with the g.s. which must be summed to the first order one-phonon coupling. Within the harmonic-vibrational model [19]) the second-order terms must have an amplitude equal to $\beta_0'' = 0.63\beta_2^2$ and to $\beta_1'' = 1.01\beta_2\beta_3$ for 0^+ and 1^- states, respectively. The largest transition amplitudes have been found for the transitions leading to the 1^- state at 3.42 MeV in ^{142}Nd and to the 1_1^- state in ^{144,146,148,150}Nd. They are of the order of 0.01 and correspond to about

$\frac{1}{4}$ of the two-phonon strength. Smaller amplitudes have been found for the other 1^- states and the 0^+ states. This result indicates that the two-phonon strength is fragmented also in the case of E0 and E1 excitations.

The 0^+ and the 1^- states seem to be equally excited in proton and deuteron scattering, as expected for isoscalar excitations. Considering therefore that the isoscalar E0 and E1 operators are of the second order, with the first-order terms leading to vanishing matrix elements as expressed by eq. (7), this implies that λ, in eq. (1), must be replaced by $(\lambda+2)$ and an extra factor of $\frac{1}{2}$ should appear in front of the integral.

In the present study the transitions to 0^+ and 1^- states have been analyzed by CC calculations, taking into account two-step processes and second-order terms. A second analysis has been performed by DWBA, considering only the direct coupling. The cross sections calculated with these two approaches have rather similar angular distributions if the DWBA calculations are performed using a second-derivative form factor and if the CC calculations are performed with the constraints on two-step and on second-order terms as given by the harmonic-vibrational model [19]). The differences in coupling amplitudes obtained in the two analyses are also rather limited, being of the order of 10–20%. Only the results from DWBA calculations are given in tables 2–6, since in this case the parametrization is much simpler. The monopole transitions are not considered in the comparisons with model predictions, because of the uncertainties found both in the experiment and in model calculations. Dipole transitions are only considered in IBM-1 calculations.

4. Strength distributions

4.1. COMPARISONS BETWEEN DIFFERENT EXPERIMENTS

A significant test of the accuracy of the method and of the actual errors in transition probabilities can be obtained comparing the results from (p, p') reaction with those from (d, d') or other data and with model evaluations. Most of the ratios $R_M = \tilde{M}_{pp}/\tilde{M}_{dd}$ have values between 0.9 and 1.40. Fluctuations in R_M values can be due to errors in the evaluation of matrix elements or to an effective dependence on the structure of the final state. In the one-fluid collective model $M_p/M_n = Z/N$ and for eqs. (3) and (4): $R_M = 1+(N-Z)/2A$. This implies that R_M should be constant for the different isoscalar transitions in a given nucleus and should display a smooth mass dependence (1.077 for $A=142$ and 1.100 for $A=150$ in Nd isotopes). This mass dependence is shown in the upper part of fig. 2 by a full line. In QPM evaluations, the proton and neutron contributions to transition probabilities change with the final state. To have a first overview of the agreement between the different experiments and model predictions we calculate the mean value of the ratio $\langle R_M \rangle$ and its variance, σ_R. The two dashed curves in fig. 2 give the QPM prediction for

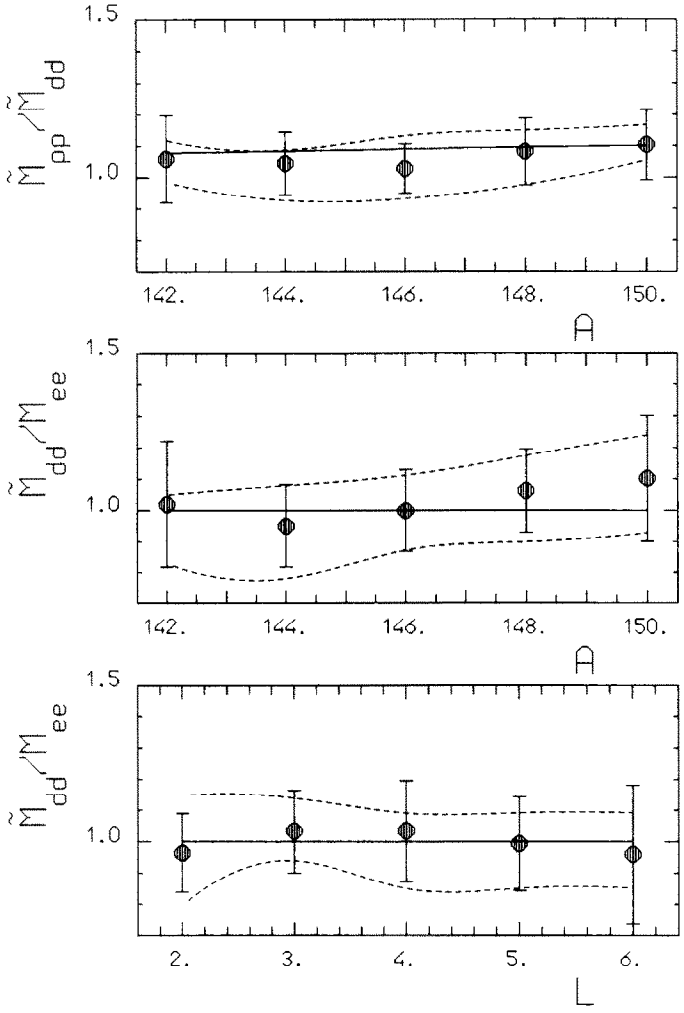

Fig. 2. Ratios of transition matrix elements from different experiments: (p, p') and (d, d') (upper part), (d, d') and (e, e') (central and lowest parts). The full curves give collective model predictions. The dashed curves give upper and lower limits of QPM predictions (see text).

the values of $\langle R_M \rangle \pm \sigma_R$, respectively. The full points give the experimental $\langle R_M \rangle$ ratios obtained from the transition matrix elements of the transitions for which both (p, p') and (d, d') cross sections have been measured. Each point gives the mean value of the whole ensemble of transition matrix elements determined for a given nucleus. The error on the point gives the variance due to the fluctuation in R_M values. It can be observed that the mean values of the QPM predictions are not far from the collective model prediction, that the experimental points lie within the limits predicted by QPM evaluations and that their values, as indicated by the error

bars, span an interval similar to that predicted by QPM evaluations. This result might be also due to the similarity of (p, p′) and (d, d′) experiments and analyses. The similarity of the method could in fact result in reduced errors in the relative values of $\tilde{M}_{pp}$ and $\tilde{M}_{dd}$ matrix elements.

The method used in the analysis of electron-scattering data is instead quite different. In principle, to compare the (p, p′) and (d, d′) with (e, e′) data, one can use the first relation in eq. (2). However, the difference $(3\tilde{M}_{dd} - 2\tilde{M}_{pp})$ has too large error to allow a significant comparison. For this reason, we consider instead the ratio $\tilde{M}_{dd}/M_{ee}$. The dashed curves again limit the region predicted by QPM evaluations. The points given in this figure have been obtained considering 60 transitions, with $\lambda = 2 \rightarrow 6$, for which (e, e′) and (d, d′) cross sections have been measured. In the central part of fig. 2 the mean experimental ratios (full points) are displayed as a function of the mass number, while in the lower part the same ratios are shown as a function of the transferred angular momentum (averaging the data belonging to final states with the same J^π value over the five nuclei). Again the agreement with model predictions is rather satisfactory. Also in this case the variance in the experimental ratios is similar to the variance of QPM evaluations. The indication is that the experimental errors and the uncertainties in the analysis do not give any clearly observable disagreement between (p, p′), (d, d′) and (e, e′) data and that the observed differences are probably due to the isovector contributions.

The lower part of fig. 2 does not display any λ-dependence of the ratio of the $M(E\lambda)$ obtained from hadron scattering and electromagnetic data. This is an interesting result since it differs from those of α-scattering experiments [20]), which implies the absence of a λ-dependence in the ratios $\sigma(p, p')/\tilde{B}_{pp}(E\lambda)$ and $\sigma(d, d')/\tilde{B}_{dd}(E\lambda)$. The different behaviour of proton- or deuteron-scattering data with respect to α-scattering data could be due to a different sensitivity to the tail of the nuclear potential.

Nuclear-resonance fluorescence experiments [21]) have been performed on the nuclei ^{142,146,148,150}Nd. Among other low-lying $J = 1$ states the level at 3.42 MeV in ^{142}Nd and the 1_1^- states in the other Nd isotopes have been observed to be relatively strongly excited, with $B_{\gamma\gamma}(E1)$ values rather constant: 0.016, 0.005, 0.014 and 0.016 $e^2\,fm^2$, respectively. Photon scattering probes the isovector strength. These E1 strengths could be due, therefore, to small but still appreciable fragments of the giant dipole isovector resonance in the 1^- low-lying states. As noted in sect. 3.4, the same states are excited by electrons and protons as well as by an isoscalar probe as a deuteron. Such result is a clear indication that electron and hadron scattering are probing the isoscalar strength. Furthermore, other phenomenological evidences indicate that the main structure of these 1^- states is due to isoscalar configurations built on the coupling of the octupole to the quadrupole degree of freedom. The excitation energy of these states is rather well correlated to the energies of the 2_1^+ and the 3_1^- states. For the strongest 1^- state in the five Nd isotopes the ratio $E(1^-)/[E(2_1^+) + E(3_1^-)]$ results to be: 0.93, 0.99, 0.83, 0.79 and 0.79, respectively.

The transition probability, $B_{dd}(E1)$ increases with the isotope mass: 0.59, 1.4, 2.6, 3.6 and 3.0 W.u. for $A = 142$, 144, 146, 148 and 150, respectively. This increase is similar to that predicted by the collective model for an E2–E3 two-phonon state. Considering β_1'', the coupling amplitude of second-order contributions obtained in the analysis discussed in sect. 3.4, and the quadrupole and octupole coupling amplitudes, β_2 and β_3, the ratio $(\beta_1''/\beta_2\beta_3)^2$, averaged over (d, d') and (p, p') data, turns out in fact to be rather constant: 0.17, 0.21, 0.17, 0.15 and 0.14 for the five isotopes, respectively.

The coupling of E3 and E2 phonons (in spherical nuclei) and of roto-vibrations in ^{150}Nd, may lead to a displacement of the charge and induce isovector dipole transitions. In this model the isoscalar and the isovector strengths should be proportional. This, however, does not seem to be the case in the Nd isotopes, considering the rather constant $B(E1)$ values found in (γ, γ') experiments. This point will be discussed also in sect. 6.4.

4.2. RELEVANT FEATURES OF THE STRENGTH DISTRIBUTIONS

The most frequent and prominent peaks in the energy spectra belong to transitions to 2^+, 3^- and 4^+ states. A large part of the E2 strength is concentrated in the 2_1^+ state, with $B_S(E2)$ values increasing from 14 W.u. for ^{142}Nd to 115 W.u. for ^{150}Nd. If the same strength is expressed in terms of the percentage of the energy-weighted sum rule (EWSR), the mass dependence is strongly reduced. In fact in all Nd isotopes the 2_1^+ state exhausts 6–7% of the EWSR and the other 2^+ states at excitation energies below E_Σ 4–5% of the EWSR. To evidence the systematic features of the data, the strength is summed over an equivalent energy range in the different nuclei up to an excitation energy: $E_\Sigma = E(3_1^-) + 2.1$ MeV, i.e. 4.184, 3.610, 3.290, 3.098 and 3.034 MeV for ^{142,144,146,148,150}Nd, respectively. As shown in fig. 3 the total E2 strength below E_Σ, exhausts a nearly constant fraction of the EWSR of 10–11%.

Also the E3 strength distribution is dominated by the first 3^- state, with transition probabilities between 22 W.u. (^{150}Nd) and 42 W.u. (^{146}Nd). The fraction of the EWSR exhausted by the 3_1^- state decreases from 7% for ^{142}Nd to 2.2% for ^{150}Nd, and that by the other 3^- states up to E_Σ increases from 1.2 to 5%. This behaviour confirms the results of a previous study: by increasing the number of valence particles the nucleus acquires collectivity and a substantial fraction of the octupole strength is transferred from the first to the other 3^- states. This interplay concerns the first and the neighbouring octupole states and not higher states, as, for instance, the low-energy octupole resonance. The comparison with model calculations gives a simple explanation of this result, at least in spherical nuclei. The E3 strength distribution at low excitation energies is fully explained as due to the fragmentation of a single f-boson (in IBM) or of the lowest E3 phonon (in QPM).

The E4 strength distributions have a more complex structure. The 4_1^+ state is the strongest E4 transition in ^{142}Nd and ^{150}Nd and has a strength comparable to that

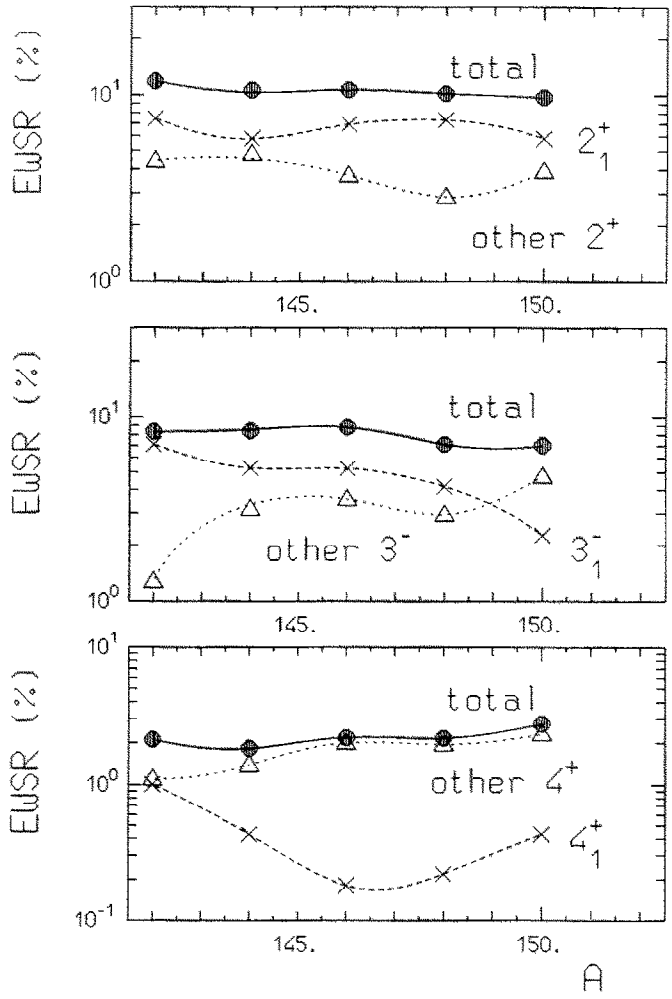

Fig. 3. Isoscalar E2, E3 and E4 strengths given as the fraction of the EWSR exhausted by the first state of each multipolarity (crosses), by the states up to the excitation energy, E_Σ, given in the text (triangles) and in total (full points).

of the second or third 4^+ state in ^{144}Nd and ^{148}Nd. In ^{146}Nd it is weaker than the second state by a factor of 2. This behaviour is connected to the evolution of the mixing of one- and two-phonon components (or sg- and dd-boson configurations in IBM). The total E4 strength exhausted below E_Σ is about 2% of the EWSR. The fragmentation is very high. In all nuclei, in fact, hexadecapole transitions are those most frequently excited in inelastic scattering below 4 MeV. Among the about 300 transitions studied in the present experiment 75 lead to 4^+ states.

5. Model calculations

5.1. THE INTERACTING BOSON MODEL

The current versions of the phenomenological IBM calculations assume s- and d-bosons as building blocks. These calculations aim to describe the low-lying even-parity states in vibrational, rotational and γ-unstable nuclei, as well as in transitional nuclei. In the intermediate cases of transitional nuclei the system is described using parameters adjusted to obtain the observed excitation energies and transition probabilities of the lowest states. If some observed states are not reproduced, the model space can be extended to include g-bosons ($\lambda = 4$), other bosons with $\lambda = 0$ and 2 (s'- and d'-bosons) and also the negative-parity bosons, p and f ($\lambda = 1$ and 3). It should be mentioned that the IBM transition operators contain terms able to transform one type of boson into another. Predicted transition rates between different states with the same number of bosons may be strong under some specific choice of model parameters.

The main drawback of the model is that it aims to describe the low-lying states with the inclusion of a very limited part of the shell-model fermion space, since the collective subspace is supposed to be entirely decoupled from the non-collective subspace of quasi-particle states. Other shortcomings are not intrinsic to the model, but are due to the approximations introduced to simplify the calculations. The model space of the present IBM analysis has been limited to valence particles outside the shell closures at $Z = 50$ and $N = 82$. Within this space we cannot describe the closed-shell nucleus ^{142}Nd. In order to describe octupole and hexadecapole states, the sd-boson model space has to be extended to include f- and g-bosons. With the introduction of these types of bosons, the hamiltonian gets very complicated. For this reason we have used the IBM-1 version of the model. This latter approximation does not distinguish between proton and neutron degrees of freedom, but is the simplest version of the IBM. One of the aims of the present study is to probe to which extent and up to which excitation energies the E1, E2, E3 and E4 strength distributions can be reproduced by IBM calculations.

The parameters of the sd-hamiltonian have been taken from the IBM-2 analysis performed by Scholten [22]) on the Sm, Gd and the heavier Nd isotopes ($A = 146$-152). These parameters can be extrapolated to ^{144}Nd with quite good results. We refer to previous papers [6,22]) for the IBM-2-sd hamiltonian and operators. To evaluate the quadrupole transition probabilities it is also necessary to use effective charges, e_2^{π} and e_2^{ν}, for proton and neutron transition matrix elements. The data considered in ref. [22]) are not very sensitive to the strength of the Majorana force. The parameters of this force and the effective charges have been determined to reproduce at the best the isoscalar and isovector matrix elements, it is to say the $\tilde{M}_{dd}$ and $2(\tilde{M}_{pp} - \tilde{M}_{dd})$ values.

Since the IBM-1 space can be regarded as a subspace of IBM-2, there is a unique way to project the operators of IBM-2 onto those of the IBM-1. The parameters of ref. [22]) projected into IBM-1 space, written as input parameters of the IBM-1 code PHINT [23]), are given in table 7. EPS is the d-boson energy. ELL, QQ, OCT and HEX are the parameters that weigh the dipole, quadrupole, octupole and hexadecapole terms, respectively. The parameter χ_Q weighs the d-boson recoupling term in the quadrupole operator: $Q^{(2)}=[(s^\dagger\tilde{d}+d^\dagger s)^{(2)}+\chi_Q(d^\dagger\tilde{d})^{(2)}]$. We refer to recent papers [5,24]) for a detailed description of IBM-1-sdf hamiltonian and operators.

TABLE 7

Parameters used in the different IBM calculations for the various Nd isotopes

Hamiltonian or operator	Parameter	^{144}Nd	^{146}Nd	^{148}Nd	^{150}Nd
IBM-2 [a])					
H_{sd}	ε (MeV)	0.95	0.90	0.70	0.47
	κ (MeV)	−0.20	−0.15	−0.10	−0.07
	χ_ν	0.6	0.0	−0.8	−1.0
	a (MeV)	0.08	0.11	0.14	0.17
T(E2)	e_2^p (e fm^2)	16.0	16.0	17.5	17.0
	e_2^n (e fm^2)	15.0	17.0	16.5	20.0
IBM-1-sd					
H_{sd}	EPS (keV)	774	683	540	353
	ELL (keV)	2.6	1.3	−0.3	−0.5
	QQ (keV)	−90.0	−71.4	−53.6	−38.9
	OCT (keV)	−0.6	1.0	1.5	1.5
	HEX (keV)	7.1	8.4	5.6	6.0
	χ_Q	−0.830	−1.342	−2.236	−2.460
IBM-1-sdf					
H_f	ε_f (keV)	1743	1448	1285	1239
V_{sdf}	FELL (keV)	15.0	10.0	4.0	0.0
	FQQ (keV)	−53.0	−45.0	−37.0	−30.0
	FEX (keV)	−1.0	0.0	0.0	6.0
T(E1)	e_1 (e fm^3)	5.2	4.9	4.7	4.5
	χ_1	0.5	0.5	0.5	0.5
T(E3)	e_3 (e fm^3)	256	248	240	232
	$\chi_{sd}=\chi_{dd}$	0.118	0.158	0.197	0.230
	χ_{df}	−2.15	−2.00	−1.85	−1.70
IBM-1-sdg					
H_g	ε_g (MeV)	1.95	1.65	1.53	1.20
V_{sdg}	ζ (MeV)	0.3	0.3	0.1	0.1
T(E4)	e_4^{dd} (e fm^4)	1920	1480	970	1200
	e_4^{sg} (e fm^4)	180	210	240	120
	e_4^{dg} (e fm^4)	610	610	610	610
	e_4^{gg} (e fm^4)	40 000	40 000	40 000	240 000

[a]) The other IBM-2 parameters have been fixed, for all the isotopes, to the values: $\chi_\pi=-1.2$, $C_0^\pi=0.4$, $C_2^\pi=0.2$, $C_4^\pi=C_0^\nu=C_2^\nu=C_4^\nu=0$.

In ref. [5]) the E3 strength distributions in ^{146,150}Nd were successfully described, using f-boson parameters that can be extrapolated to the other Nd isotopes. The parameters necessary to describe the octupole degree of freedom are the f-boson energy (ε_f), the parameters that define the two-body interaction of the f-boson with the sd-bosons (FELL, FQQ and FEX: dipole, quadrupole and exchange interactions) and the effective charges entering into the T(E3) transition operator:

$$T(\mathrm{E3}) = e_3\{(s^\dagger\tilde{f} + f^\dagger s)^{(3)} + \chi_{\mathrm{df}}(d^\dagger\tilde{f} + f^\dagger\tilde{d})^{(3)} + [\chi_{\mathrm{sd}}(s^\dagger\tilde{d} + d^\dagger s)^{(2)} + \chi_{\mathrm{dd}}(d^\dagger\tilde{d})^{(2)}][(s^\dagger\tilde{f} + f^\dagger s)^{(3)}]\}\,. \tag{8}$$

To reduce the ambiguities of the best-fit procedure all these parameters, as shown in table 7, have been taken with a smooth mass dependence. The effective charges have been restricted to the values obtained from semiempirical rules: $\chi_{\mathrm{sd}} = \chi_{\mathrm{dd}} = \beta_2$ and $e_3 = 128(Z/A)[(\Omega - N_b)/\Omega]^{1/2}$. Where N_b is the number of bosons considered for each nucleus and Ω is the maximum number of bosons in the valence orbitals considered [5]).

The E1 strength distributions are analyzed assuming that the low-lying 1^- states are due to the recoupling of the f-boson with the sd-bosons. The p-boson is not considered and no further adjustments of the sdf-hamiltonian have been performed to better reproduce 1^- states data. We have assumed a dipole operator, T(E1), with the following form:

$$T(\mathrm{E1}) = e_1\{(d^\dagger\tilde{f} + f^\dagger\tilde{d})^{(1)} + \chi_1[(s^\dagger\tilde{d} + d^\dagger s)^{(2)} + \chi_2(d^\dagger\tilde{d})^{(2)}] \times [(s^\dagger\tilde{f} + f^\dagger s)^{(3)}]^{(1)}\}\,. \tag{9}$$

To limit the number of parameters we have taken $\chi_1 = 0.5$ and $\chi_2 = \chi_Q$.

The E4 strength predicted by the IBM model in the basic sd-approximation is mostly concentrated in one 4^+ state, usually located at an excitation energy near to that observed for the 4_1^+ state. This strength is due to the d-boson recoupling. The inclusion of the g-boson (sdg-expansion) allows new $\lambda = 4$ configurations due to sg, dg and gg pairs and thus facilitates the interpretation of a further part of the experimental E4 strength distribution. A previous study on vibrational nuclei with masses $A = 94$–112, has evidenced the clustering of the hexadecapole strength into groups that have been tentatively identified with those predicted by the IBM-1-sdg model [6]). Among the several additional parameters connected to the g-boson, we have used the g-boson energy, ε_g, and the parameters γ, ζ and η that define the interaction between the g- and the sd-bosons. More specifically the additional terms in the sdg hamiltonian have been limited to the following terms:

$$\varepsilon_g[g^+\tilde{g}]^{(0)} + \gamma[(g^+\tilde{g})^{(2)}(d^+\tilde{d})^{(2)}]^{(0)} + \zeta[(g^+s^+)^{(4)}(\tilde{d}\tilde{d})^{(4)} + (d^+d^+)^{(4)}(\tilde{g}\tilde{s})^{(4)}]^{(0)} + \eta[(d^+\tilde{d})^{(4)}(s^+\tilde{g} + g^+s)^{(4)}]^{(0)}\,.$$

The transition operator, $T(E4)$, can be parametrized by 4 polarization charges (e_4^{dd}, e_4^{sg}, e_4^{dg}, e_4^{gg}), that weigh, respectively, the contributions coming from the dd, sg, dg and gg terms (DD, SG, DG and GG configurations).

These parameters were adjusted to reproduce the experimental strength distributions. The parameter ε_g shifts the excitation energy of the 4^+ states belonging to the SG, DG and GG configurations. The parameter γ influences the relative energies of the different g-boson configurations. The best agreement with the experiment is obtained with $\gamma = 0$. The parameters ζ and η have a weak influence in the level energies, but generate both mixing and splitting of g- and sd-boson configurations. Since these two parameters give equivalent effects, we kept $\eta = 0$ and adjusted the ζ-values. The resulting parametrization of the g-boson part of the hamiltonian is given in table 7 and turns out to have a smooth mass dependence. However, the choice of the effective charges to be used in the transition operator $T(E4)$ is still an open question. To estimate these parameters in the E4 operator one can use a microscopic model for the g-boson. As discussed in ref. [25]), at the zeroth-order of very simple models (single j-shell model or harmonic oscillator), the four g-boson effective charges should be of the same order. This result is coming out only in part from a best-fit procedure of the experimental E4 strength distributions. The values of e_4^{dd} and e_4^{dg} are in fact of the same order of magnitude, but the experiment clearly requires e_4^{sg} values much smaller than e_4^{dd} (by a factor of 4–10). Moreover some improvement at high excitations is obtained using very large and probably unphysical e_4^{gg} values. The comparison with the experiment is discussed in sect. 6.

5.2. THE QUASI-PARTICLE PHONON MODEL

Excited vibrational states of even-even nuclei are treated by the QPM in terms of phonon creation operators built upon the wave function of the ground state which is considered as a phonon vacuum. Phonons Q^+ are introduced as a linear combination of pairs of quasi-particle creation α^+ and annihilation α operators as follows:

$$Q^+_{\lambda\mu i} = \tfrac{1}{2} \sum_{jj'}^{N,Z} \{\psi^{\lambda i}_{jj'}[\alpha^+_{jm}\alpha^+_{j'm'}]_{\lambda\mu} + (-1)^{\lambda-\mu}\phi^{\lambda i}_{jj'}[\alpha_{jm}\alpha_{j'm'}]_{\lambda-\mu}\} \tag{10}$$

for spherical nuclei, where $jm \equiv |n, l, j, m\rangle$ are the shell quantum numbers of a spherically symmetric average field, and

$$Q^+_{Ki\sigma} = \tfrac{1}{2} \sum_{q_1 q_2} \{\psi^{Ki}_{q_1 q_2} A^+(q_1 q_2; K\sigma) - \phi^{Ki}_{q_1 q_2} A(q_1 q_2; K-\sigma)\} \tag{11}$$

for deformed nuclei. Single-particle states of an axially symmetric average field for deformed nuclei are characterized by the quantum numbers q and σ, where $\sigma = \pm 1$ and q equals the angular-momentum projection onto the symmetry axis of the

nucleus K, parity π and asymptotic quantum numbers $Nn_z\Lambda\uparrow$ at $K=\Lambda+\frac{1}{2}$ and $Nn_z\Lambda\downarrow$ at $K=\Lambda-\frac{1}{2}$. In eq. (11) we have used the following notations:

$$A^+(q_1q_2;\,K\sigma)=\begin{cases}\sum_{\sigma'}\delta_{\sigma'(K_1-K_2),\sigma K}\,\sigma'\alpha^+_{q_1\sigma'}\alpha^+_{q_2-\sigma'} & \text{if} \quad |K_1-K_2|=K\\ \sum_{\sigma'}\delta_{\sigma'(K_1+K_2),\sigma K}\,\alpha^+_{q_2\sigma'}\alpha^+_{q_1\sigma'} & \text{if} \quad K_1+K_2=K,\end{cases} \tag{12}$$

all $K\geqslant 0$. Quasi-particle operators result from the canonical Bogoliubov transformation of particle and hole creation operators. For the occupation numbers and position of the Fermi surface we solve the BCS equations for protons and neutrons.

The phonon spectrum and the structure coefficients ψ and ϕ in eqs. (10), (11) are obtained from RPA calculations with an effective nuclear hamiltonian which includes an average field for neutrons and protons, a pairing interaction and a multipole residual interaction of separable form with the Bohr–Mottelson radial dependence, i.e. the derivative of the central part of the average field.

In the present paper the excited states of the deformed isotope ^{150}Nd are treated within the one-phonon approximation. The states with $I^\pi K=2^+2$, 4^+2 and the corresponding B(E2) and B(E4) values are calculated with quadrupole and hexadecapole interactions. The parameters of the axially symmetric Woods–Saxon potential for the average field have been taken from ref. [26]). We have used monopole and quadrupole pairing, isoscalar and isovector particle-hole and particle-particle channels of the residual interaction. Parameters of the residual interaction have been adjusted to reproduce the properties of the lowest state for each K^π. The explicit expressions of the RPA equations and the parameters of the residual interaction used in the case of deformed nuclei can be found in ref. [9]).

For the spherical isotopes ^{142,144}Nd and transitional ^{146}Nd, which have been considered within this model in the spherical picture, we have used the results of structure calculations from a previous paper [2]) and from recent studies [4,27]). In these papers transition charge densities of low-lying excited states of these isotopes extracted from the (e, e′) cross sections were compared to the ones of the QPM calculations. Excited states were described by wave functions that include one-, two- and a limited number of three-phonon configurations. The description of the proton part of nuclear excitations was rather successful in general. Thus, in the present calculations, we have kept the same scheme and the values of the adjusted parameters. We refer the reader to ref. [2]) for other details. The experimental data from the present experiments will serve as a good test of both proton and neutron parts of the nuclear wave functions.

Effective charges have been used in the past to compare experimental and calculated transition probabilities. Their use compensates for the truncation of the basis states of the average field, namely in our case the neglect of unbound states. For quite heavy nuclei, like Nd isotopes, and for low-lying states we expect the role of the continuum to be not very strong and thus, the continuum can be substituted by a limited number of quasibound states. This was the motivation in ref. [2]) for not using effective charges in the analysis of transition densities in ^{142}Nd. In the

calculations for ^{142,144,146}Nd we have included all quasi-bound states with small widths as in previous calculations [2,4,27]). This inclusion, however, could not be sufficient to avoid the use of effective charges since not all the continuum space is included exactly. Test calculations for ^{142}Nd on the role of parameters such as those of the neutron potential well or the form of the effective residual interaction gave practically the same results and confirmed that the main reason for the effective charges resides in the incompleteness of the single-particle levels due to the replacement of the full continuum with only the quasi-bound states.

Calculations with single-particle spectrum from the bottom of the average field up to +50 MeV with effective charges equal to $e_p = 1.0e$ and $e_n = 0$ give almost the same B(E2) and B(E3) values as the calculations with the truncation of levels above +5 MeV and $e_p = 1.2e$ and $e_n = 0.2e$. Equivalent effective charges, to compare with isoscalar mass transition matrix elements, should be $e_p = e_n = 1.2e$. Some small variations of effective charges for proton and neutron excitations are possible since we cannot expect the same role of the continuum for both type of excitations.

To avoid the use of different effective charge values for each single isotope, that is to say to avoid the use of the effective charges as additional adjustable parameters, one can take the same charge values for a chain of isotopes. As shown below evidence of a mass dependence of the effective charges is obtained only in the case of the transitions to the 2_1^+ and to the 3_1^- states. Finally the effective charges have been fixed, for all the nuclei considered in QPM calculations, to $e_p = 1.1e$ and $e_n = 1.3e$. This choice will be discussed in sect. 6.6.

The nucleus ^{148}Nd is out of the scope of this approach. In fact in transitional nuclei it must be taken into account that the shape of the average field is unstable and varies, in principle, with each nuclear state. In our approach the average field, spherical or deformed, is fixed. Also all the correlations mentioned above are extremely strong and can be hardly included very accurately.

In the comparisons of the QPM calculations with the experimental data, monopole and dipole transitions will not be considered; the former because their description in spherical nuclei is expected to be incomplete since particle–particle correlations were not taken into account in the residual interaction and the latter because of difficulties connected mainly with the complex structure of the final states. The low-lying 1^- states of spherical Nd isotopes have in fact a two-phonon nature like $[2_1^+ \times 3_1^-]^{(1)}$, $[4_1^+ \times 3_1^-]^{(1)}$, $[4_1^+ \times 5_1^-]^{(1)}$, etc. A good description of E1 strength distributions requires then an increase of the three-phonon basis, since, in contrast with the angular-momentum transfers with $\lambda \geqslant 2$, the leading configurations are no more the one- and two-phonon configurations but the two- and three-phonon ones.

The low-lying 1^- states in deformed nuclei, contrary to spherical nuclei, have a one-phonon nature and are generated mainly by the isoscalar octupole residual interaction. The E1 transition probabilities to $J^\pi = 1^-$ and $K = 0, 1$ vibrational states in strongly deformed nuclei have been calculated within the QPM, taking into account isoscalar and isovector octupole and isovector dipole residual interaction [28]).

In the case of ^{150}Nd we have concentrated the efforts on the description of the 2^+, 3^- and 4^+ vibrational states. Nevertheless the QPM should, in principle, be able to describe also other multipolarities.

6. Comparisons with model calculations

In this section the experimental strength distributions are compared with theoretical evaluations. QPM evaluations have been performed for the transitions with $\lambda = 2$ to 6 in ^{142,144,146}Nd and those with $\lambda = 2, 3$ and 4 in ^{150}Nd. The results of IBM calculations concern transitions with $\lambda = 1$ to 4 in ^{144,146,148,150}Nd. The results of these calculations are shown in figs. 4–15. In all the figures the experimental strengths are given as full points and the calculated values are displayed as vertical dashed lines. To better appreciate the agreement in the gross structure of each strength distribution, both experimental and calculated values are also represented as overlapping peaks after smearing with a gaussian function of 200 keV f.w.h.m.

6.1. QUADRUPOLE TRANSITIONS

Several 2^+ states have been found: from a minimum of 5 states in ^{148}Nd to a maximum of 16 in ^{146}Nd. In fig. 4 the results of IBM-2 calculations are compared with the experiment. The strength of the first and in some cases of the second state is well reproduced, but not the strengths of transitions to higher-lying 2^+ states that are generally underestimated. The IBM states, in the high-energy region, are of mixed-symmetry type and have a dominant isovector component since the proton and neutron matrix elements are similar in absolute value but with opposite sign. Their location in excitation energy depends strongly on the Majorana force, while their isoscalar transition probability is not negligible only assuming proton and neutron effective charges with quite different values. With the parameters of the Majorana force of ref. [22]) ($\xi_1 = \xi_2 = \xi_3 = a = 0.06$) these states are located at excitation energies around 2 MeV. To improve the agreement with the experiment one can assume a stronger Majorana force for the heaviest isotopes ($a = 0.08 \rightarrow 0.17$ for ^{144}Nd$\rightarrow$ ^{150}Nd). However, clear improvements are obtained in level positions but not in strength values. It should be noticed that further adjustments in the model parameters are limited by the overall behaviour of the experimental isoscalar and isovector matrix elements (figs. 4 and 5). A larger difference between proton and neutron effective charges would improve the agreement with the isoscalar transition strengths but would be in contrast with the isovector matrix elements. In spite of their poor quality, the experimental data on the isovector components are of some importance in the comparison with model predictions.

The results of QPM evaluations are shown in fig. 6. The experimental distribution is quite well reproduced in ^{142}Nd and ^{144}Nd. The agreement is less satisfactory, but still acceptable in ^{146}Nd. This less satisfactory agreement could be due to the

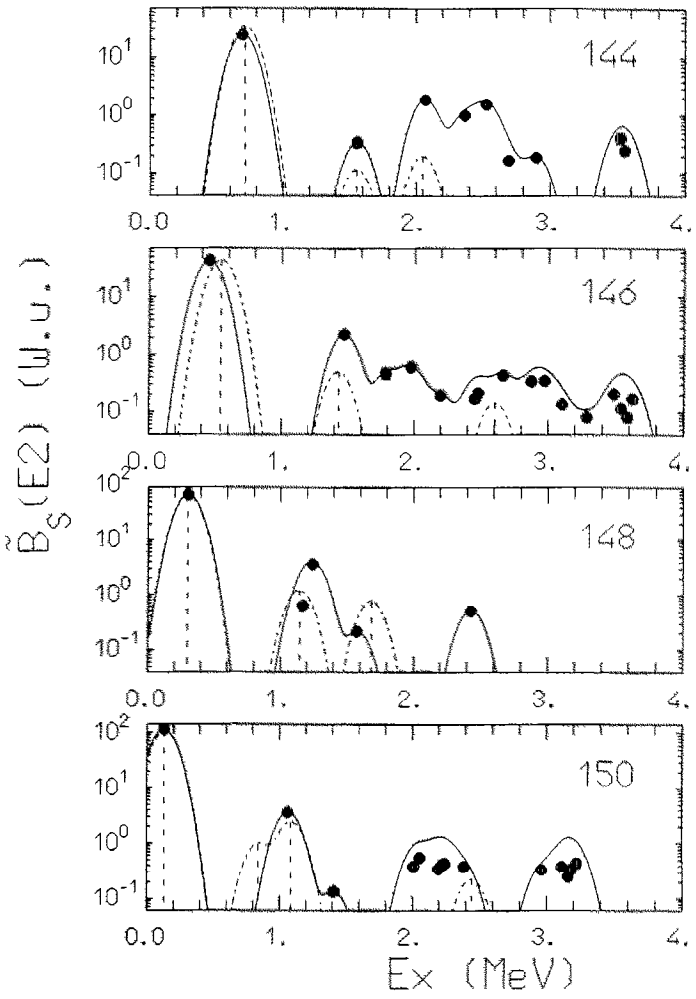

Fig. 4. Experimental isoscalar E2 strengths (full points) compared with IBM-2 evaluations (vertical dashed lines). To better appreciate the agreement in both the energy positions and the strength values, the data and the IBM-2 evaluations are also represented as overlapping distributions after smearing with a 200 keV wide gaussian function (full and dash-dotted curves, respectively).

difficulties connected with the strong coupling between one-, two- and three-phonon configurations. This strong coupling requires the inclusion of as many configurations as possible, but, to limit computing time, a truncation of the phonon basis was necessary. This includes all the one-phonon configurations with excitation energy below 3.2 MeV, two-phonons below 5.5 MeV and the three-phonons from only the first 2^+, 3^-, 4^+ and 5^- one-phonon terms. Such a basis truncation might limit the validity of the calculation.

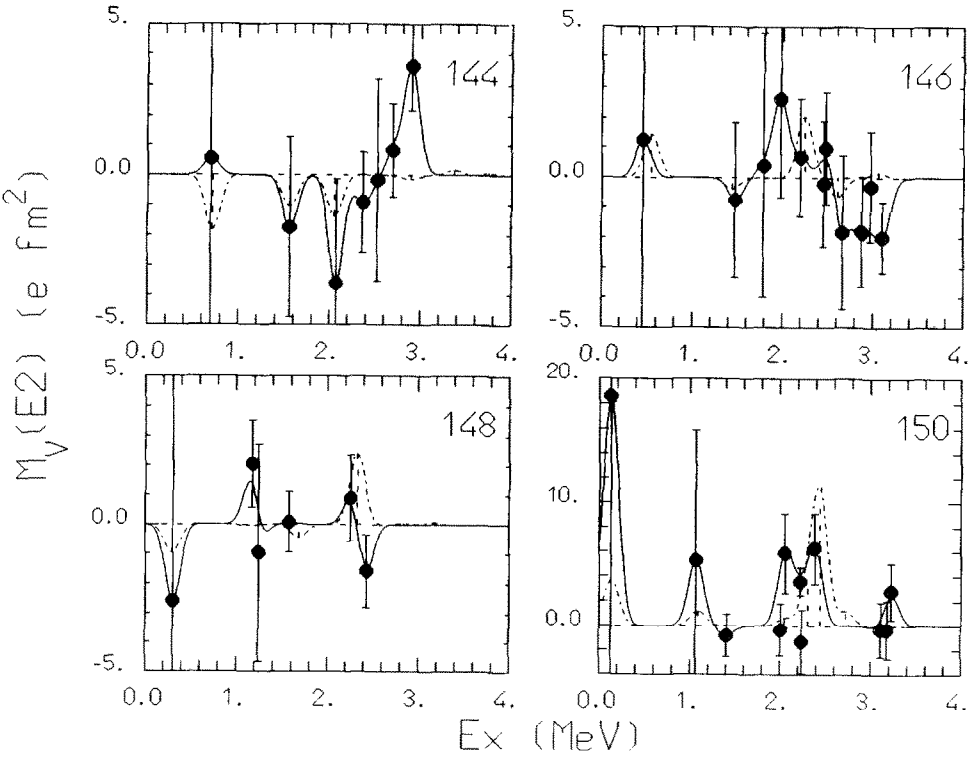

Fig. 5. Same as fig. 4 for E2 isovector matrix elements.

In the present QPM calculations the parameters of the quadrupole residual interaction have been fixed to reproduce the experimental excitation energy of the first 2^+ state. This prescription results in a weaker increase of the $B(E2)$ value through the chain than that observed in the experiment. As shown below, a similar result is obtained in the case of other strong collective transitions as those to the 3_1^- levels or to some 4^+ state.

In ^{142}Nd the first four 2^+ states have a quite pure one-phonon configuration. The first two-phonon state $[2_1 \times 2_1]^{(2)}$ is located at 3.195 MeV. The group of states, located between 4 and 5 MeV, contains several two-phonon configurations: $[2_1 \times 4_1]^{(2)}$, $[2_1 \times 4_2]^{(2)}$, $[2_1 \times 2_3]^{(2)}$, $[3_1 \times 3_1]^{(2)}$, etc. Even in ^{144}Nd the first four one-phonon configurations generate rather pure 2^+ states (2_1^+, 2_3^+, 2_4^+, 2_5^+). The two-phonon $[2_1 \times 2_1]^{(2)}$ state can be identified with the experimental 2_2^+ state. The structure of the 2^+ states in ^{146}Nd is in general more complex, with a strong mixing of different multi-phonon configurations. For instance the wave function of the 2_1^+ state has 73% of one-phonon components and 22% and 4% of two- and three-phonon components, respectively. For the 2_2^+ state the percentages of the same configurations are 8%, 56% and 33%, respectively.

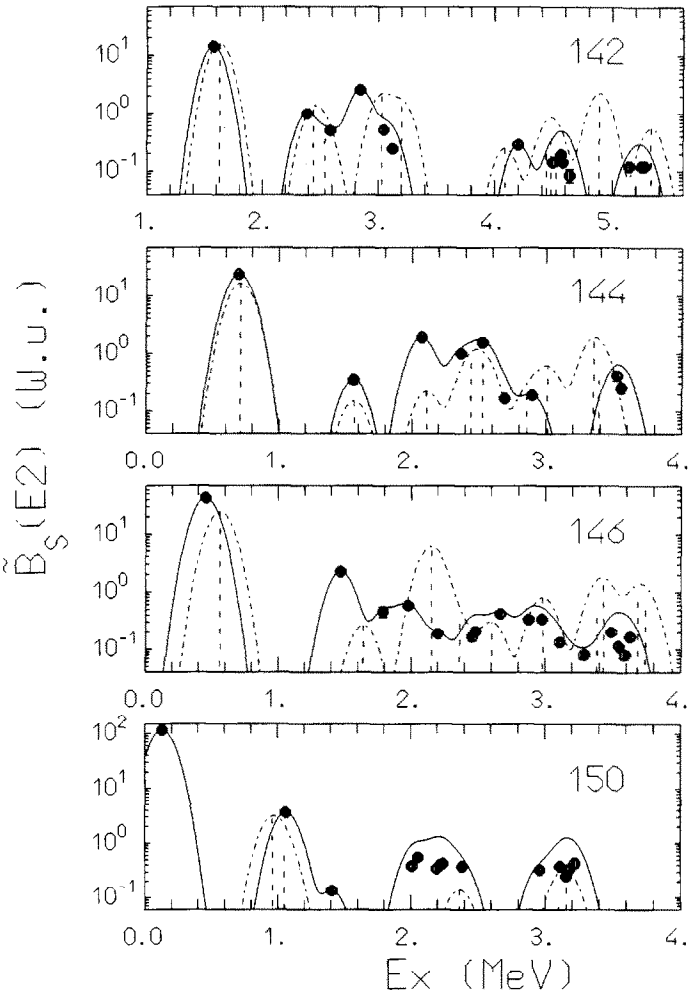

Fig. 6. Experimental E2 strengths (full points and curves) compared wtih QPM evaluations.

In ^{150}Nd the first 2^+ is a rotational state and is not described by the model. QPM predicts one-phonon states with position and strength in agreement with a part of the observed transitions. Two levels located around 1 MeV have K^π values equal to 2^+ and 0^+ and can be identified with the second and third experimental 2^+ states. Several other 2^+ states are predicted below 4 MeV; those with an observable strength have $K^\pi = 2^+$ and are located at excitation energies of about 2.4 and 3.1-3.2 MeV.

The E2 strength distributions predicted by QPM are due to, at least, six quadrupole phonons. Their strength is modified and in some cases split by the mixing with two-phonon configurations in spherical nuclei and by the deformation in ^{150}Nd. These six one-phonon configurations are located at excitation energies below

3.2 MeV. The failure of IBM-2 calculations at excitation energies above the second 2^+ state is evidently due to the fact that only one type of d-boson is considered. This points out the necessity of other, higher-lying, $\lambda = 2$ bosons.

6.2. OCTUPOLE TRANSITIONS

Figs. 7 and 8 give the comparison between experimental and calculated E3 strengths. The number of 3^- states predicted by IBM-1-sdf and QPM calculations, with an observable strength, is not as high as in the experiment, however the gross structure of the distribution is fully reproduced. The better agreement found with

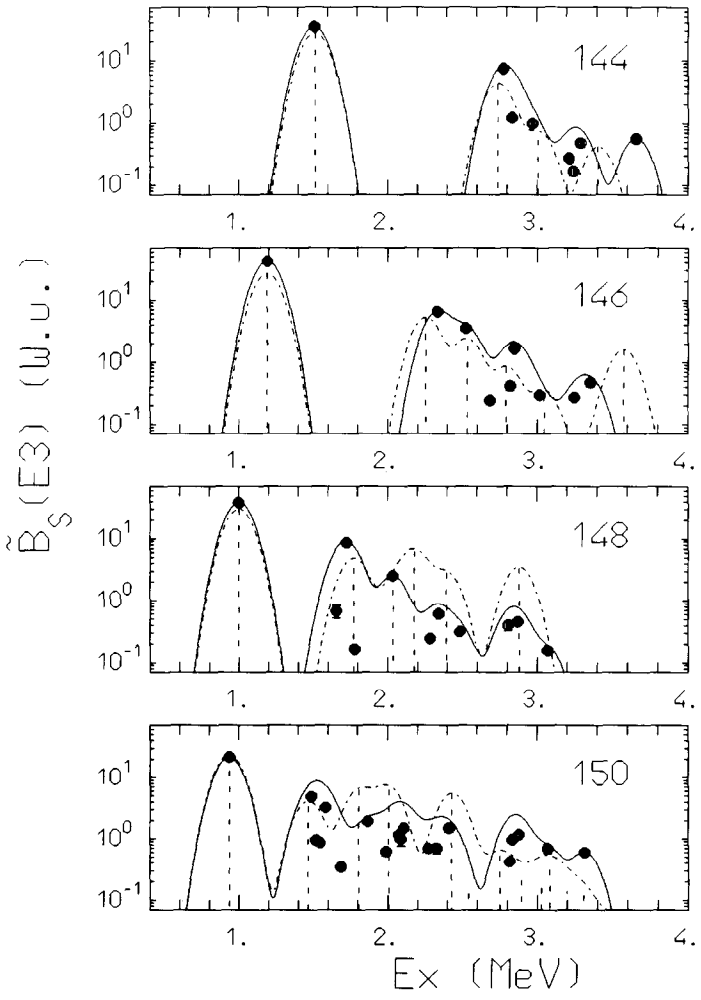

Fig. 7. Experimental E3 strengths (full points and curves) compared with IBM-1-sdf evaluations (dashed lines and dash-dotted curves).

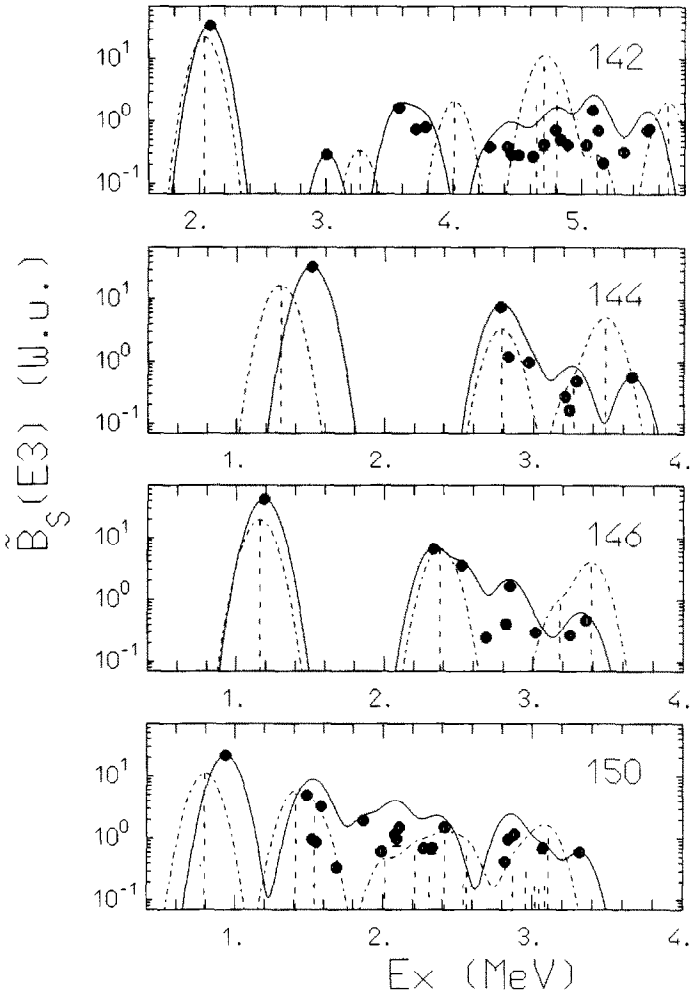

Fig. 8. Experimental E3 strengths (full points and curves) compared with QPM evaluations (dashed lines and dash-dotted curves).

IBM calculations should not be emphasized because of the larger number of adjustable parameters in the sdf-version of IBM-1 than in QPM. The most evident failure of the QPM concerns the strength of the first 3^- states, which is in general predicted too low. Moreover, it should be remarked (fig. 8) that the QPM progressively underestimates the strength of these states along the isotopic chain. The main reason for this tendency is the same as for the 2_1^+ states, but there is some further feature specific of the octupole strength in the $N = 82$ region. The shell closure at $N = 82$ is affecting more the E3 excitations since they cannot be obtained by inner shell transitions. The set of parameters used in the present analysis cannot be easily

improved. In fact it is possible to increase the collectivity of the first E3 one-phonon configuration and this improves the agreement with the experimental $B(E3)$ values but this would create problems resulting in a too low location of the first 2^+ and 4^+ states. This result is due to the coupling of the first 2^+ one-phonon configuration with the E3–E3 two-phonon configuration, $[3_1^- \times 3_1^-]^{(2)}$. This coupling is very strong and depends sensitively on the collectivity of both one- and two-phonon configurations. The same is found for the 4^+ states generated by the first E4 one-phonon configuration.

The fact that IBM and QPM give equivalent descriptions to the experiment can be easily understood, at least in the lighter isotopes. IBM-1-sdf describes the low-lying 3^- states as the fragmentation of the strength of only one f-boson through the df or sd · sf operators. Similarly, in spherical nuclei, QPM describes the same states as the fragmentation of the first E3 one-phonon state due to the mixing with the lowest two-phonon states: $[2_1 \times 3_1]^{(3)}$, $[2_1 \times 5_1]^{(3)}$, $[3_1 \times 4_1]^{(3)}$, $[3_1 \times 6_1]^{(3)}$, etc. It is to say, the similarity of the QPM results with those of the IBM is due, in spherical nuclei, to the fact that the contributions coming from the second and higher E3 one-phonon states are negligible below 3.2–3.5 MeV excitation energy.

In ^{150}Nd the fragmentation of the E3-phonon strength is instead due to the deformation and involves not only the lowest one-phonon configuration. The strength distribution in ^{150}Nd is determined by the positions of the different K^π bands, that can be mixed. As shown in fig. 8, the gross structure of octupole strength in this nucleus displays 4 different bumps located around 0.8, 1.45, 2.4 and 3.1 MeV. These bumps are due to one or more states that in the QPM calculations have K^π values equal to: 0^-, $(1^-, 2^-)$, $(3^-, 1^-, 0^-, 1^-, 2^-)$, $(3^-, 2^-, 1^-, 3^-, 0^-, 2^-, 3^-)$, respectively. It can be remarked that, in deformed nuclei, IBM-1-sdf and QPM calculations give similar strength distributions, but with a different description of the octupole states. This difference lies in the fact that in IBM-1-sdf the octupole strength is strongly fragmented but still belongs to the unique f-boson, in the QPM the octupole strength is due to a large number of one-phonon states with a different quasi-particle structure. This different quasi-particle structure could be tested in principle by one-nucleon transfer reactions and β-decay measurements.

6.3. HEXADECAPOLE TRANSITIONS

The comparison between calculations and experimental data is given in figs. 9 and 10. IBM-1-sdg reproduces the strength of the low-lying 4^+ states. The strength of the states lying above 2.2 MeV is less satisfactorily reproduced. The overall agreement with the experiment is better in the case of QPM calculations. In QPM the E4 strength distribution below 4 MeV is due to six E4 one-phonon states. This is similar to the situation in the E2 strength distribution and suggests the inclusion in IBM-1 calculations of other d- and g-bosons, lying higher in excitation energy. The first 4^+ state predicted by IBM-1-sdg is mainly due to the d-boson recoupling

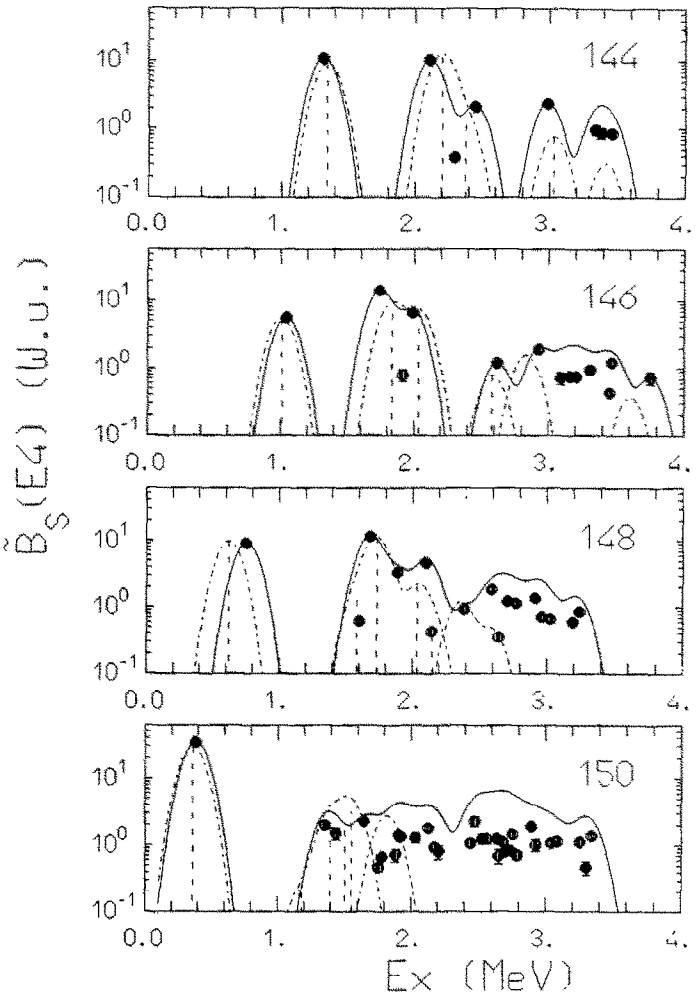

Fig. 9. Experimental E4 strengths (full points and curves) compared with IBM-1-sdg evaluations (dashed lines and dash-dotted curves). The dash-dotted curves, without a vertical dashed line, indicate transitions with a dominant GG contribution (see text).

and can be identified with the 4_1^+ experimental state. The other prominent transitions are due to the SG configuration and can be identified with the second state in ^{144,146}Nd, with the third state in ^{148}Nd and the fourth in ^{150}Nd. Other 4^+ states have a more complex structure and are due to the mixing of DD, DG and GG configurations. In fig. 9, the dash-dotted curves without a vertical dashed line indicate transitions with a dominant GG contribution, that is obtained using a very large e_4^{gg} effective charge. The need for so large effective charges could be due to the use of a too limited model space, it is to say to the need of introducing more g-bosons. This probably sets a limit in the excitation energy at which the hexadecapole strength

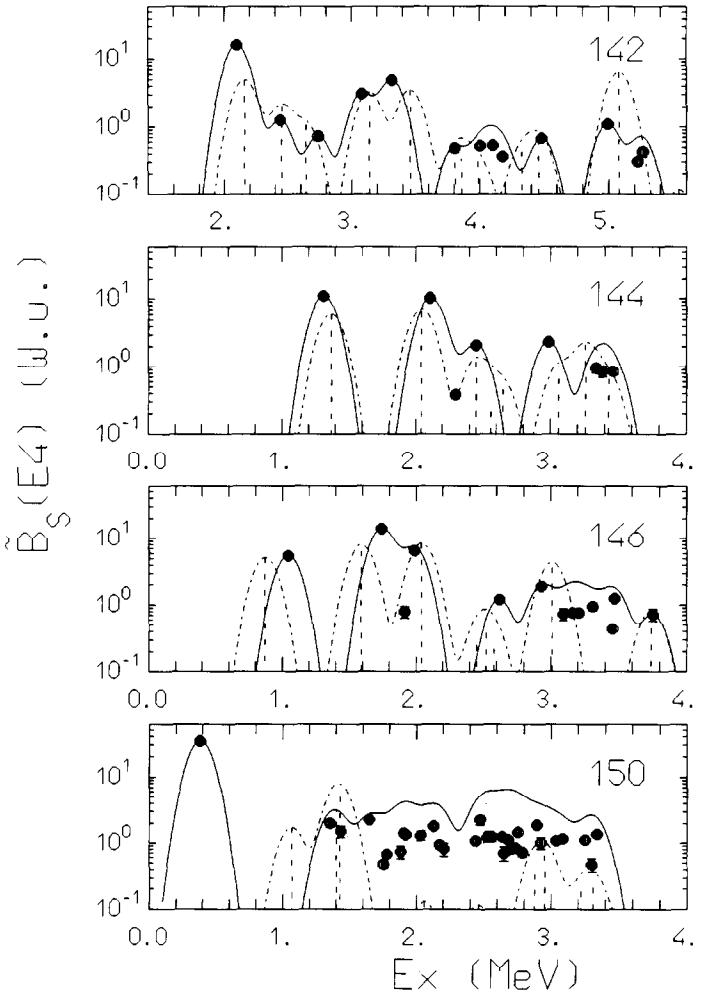

Fig. 10. Experimental E4 strengths (full points and curves) compared with QPM evaluations (dashed lines and dash-dotted curves).

can be reproduced with only one g-boson to 3.6 MeV in ^{142}Nd and to only 1.7 MeV in ^{150}Nd.

It is worth noting that the QPM distributions are due to several one-phonon configurations with large effects arising from the mixing between one- and two-phonon configurations. For instance, the 4_4^+ and the 4_5^+ states in ^{142}Nd are due to the splitting of the fourth E4 phonon caused by the mixing with the $[2_1 \times 2_1]^{(4)}$ two-phonon state. The 4_1^+ and the 4_2^+ states in ^{144}Nd are due to the splitting of the first E4 phonon due to mixing with the same two-phonon state. In ^{146}Nd again the first E4 phonon is split, but as a result of the mixing with the $[2_1 \times 4_1]^{(4)}$ two-phonon

state and should correspond to the second and fourth experimental 4^+ states. The weak 4_3^+ state found in the experiment is missed in QPM. The three-phonon configurations play a role strongly increasing with the mass. The three-phonon component in the wave functions of the different 4^+ states is always below the 10% level in ^{142}Nd, is of the order of 10–20% in several 4^+ states in ^{144}Nd and reaches 31%, 21% and 22% in the 4_1^+, 4_2^+, 4_6^+ states in ^{146}Nd, respectively.

The large and increasing complexity of the 4^+ states in ^{142}Nd, ^{144}Nd and ^{146}Nd has two main reasons: the increasing collectivity of the first E4 one-phonon configuration and the decreasing gap between one- and two-phonon configurations. In fact the first E4 one-phonon in these nuclei has its energy very close to the two-phonon configuration $[2_1^+ \times 2_1^+]$. A different situation, with a larger gap, is found in the case of the E2 and E3 one-phonon and the respective two-phonon configurations. This is the reason of the larger mixing observed between one- and two-phonon configurations in the case of 4^+ states in comparison to the 2^+ and 3^- states.

In ^{150}Nd the first 4^+ state is rotational in character and is not described by the model. The intrinsic, vibrational states, with a sizeable strength are located at the beginning ($\sim$1.3 MeV) and at the end (3–4 MeV) of the observed strength distribution. Both groups include $K^\pi = 2^+$, 3^+ and 4^+ states.

6.4. DIPOLE TRANSITIONS

Recently the E1 γ-ray transitions between low-lying states in rare-earth nuclei (Sm, Gd, Dy isotopes) have been compared with IBM-sdf calculations [29,30]). To reproduce the experimental results, two-body terms have been included in the transition operator, $T(\mathrm{E1})$. The second term in eq. (9) is one of the possible forms of these two-body operators. The leading contributions to the E1 strength are coming from the first and second terms in eq. (9), due to df and sd · sf coupling, respectively (one- and two-body terms in the formalism used by Von Brentano *et al.* [29,30]). These two terms give very similar strengths distributions and, therefore, equivalent results are obtained using different χ_1 and e_1 values. The calculated curves given in fig. 11 have been obtained assuming $\chi_1 = 0.5$. This value is consistent with solution 1 given in table 2 of ref. [29]). A second solution is used in refs. [29,30]), with a small and negative value of χ_1, of the order of -0.05. This solution seems less appropriate to the data considered here since it leads to a nearly complete destructive addition of the two main terms in the calculated strength for the 1_1^- state, which, as a result, will have a transition strength too weak in comparison with the experiment. The IBM-1-sdf, with the simple parametrization given in table 7, seems able to reproduce the position and the intensity of the transition, leading to the first 1^- state. Also the second 1^- state is reproduced, at least as far as the excitation energy is concerned. It can be remarked that the strong mass dependence of the transition probability $\tilde{B}_{\mathrm{dd}}(\mathrm{E1})$ is reproduced by IBM-1-sdf calculations with a constant (actually slightly decreasing) dipole effective charge, e_1.

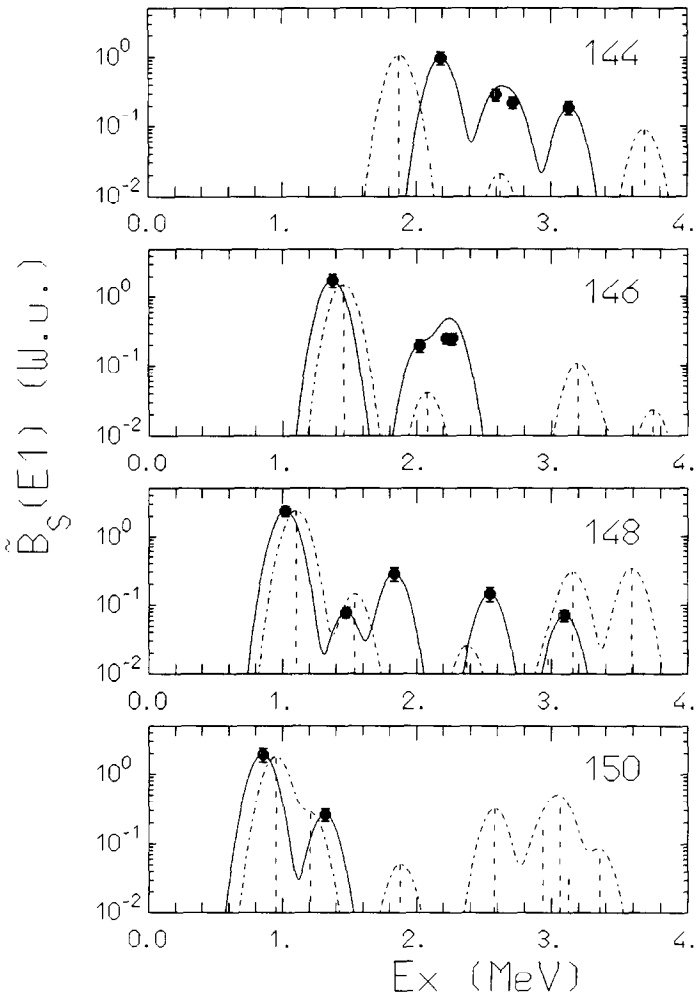

Fig. 11. Experimental E1 strengths (full points and curves) compared with IBM-1-sdf evaluations (dashed lines and dash-dotted curves).

As discussed in sect. 4.2 the E1 strength detected in the present experiment is proportional to $(\beta_2\beta_3)^2$ and is of isoscalar type. With respect to the other experiments here cited, we have two opposite evidences. The fact that γ-decay experiments are well described by a model which does not distinguish between proton and neutron degrees of freedom (IBM-1-sdf) and with parameters similar to those obtained in the present analysis, suggests that the excited states considered (with different spins and parities) have large quadrupole-octupole configurations with isovector E1 transition strengths proportional to the isoscalar strengths predicted by the model. The fact that the E1 strength, obtained from the (γ, γ') excitation of the low-lying

1^- states in Nd isotopes, does not depend on $(\beta_2\beta_3)^2$, suggests instead the presence of isovector components, connected to shell effects [31]).

6.5. OTHER MULTIPOLARITIES

The E5 strengths in ^{142,144,146}Nd are shown in fig. 12, where they are compared with QPM predictions. The agreement is quite satisfactory and somehow unexpected. In fact for the 5^- and higher-multipolarity states the QPM has some shortcomings. The approximation used to treat the continuum is even more crude for these states. Other difficulties are found in the procedure used to fix the parameters of the effective residual interaction. These parameters are adjusted to reproduce the excitation energy and the collectivity of the lowest state of each multipolarity, which is

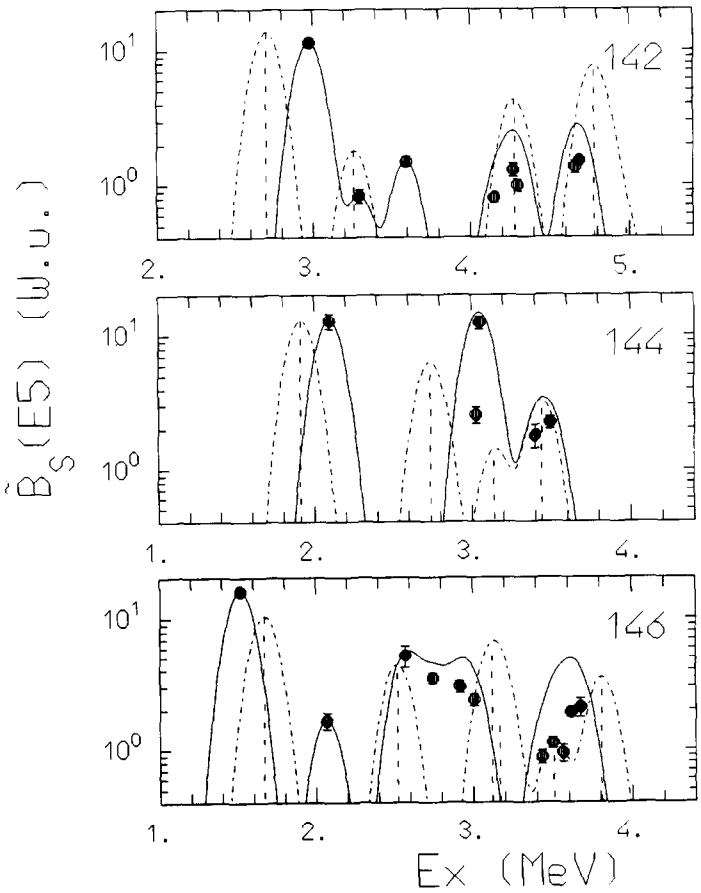

Fig. 12. Experimental E5 strengths (full points and curves) compared with QPM evaluations (dashed lines and dash-dotted curves).

mainly built from a single one-phonon configuration. However, the high multipolarity states are less collective and contain significant admixtures of two- and three-phonon components, thus making their excitation energy more sensitive to the quasi-particle level scheme and less to the parameters of the force. Hence, *a priori*, one should expect only a schematic agreement with the experiment. Nevertheless not only the E5, but also the E6 strength distributions are quite satisfactorily reproduced, with the exception of the 6^+ states in ^{142}Nd, as shown in fig. 13.

The structure of the 5^- and 6^+ states, predicted by the QPM calculations, has a marked similarity with that for the 3^- and 4^+ states, respectively. The E5 strength distribution below 4 MeV is mainly due to the first E5 one-phonon state and to its splitting due to the mixing with two-phonon configurations: $[2_1 \times 3_1]^{(5)}$, $[2_1 \times 5_1]^{(5)}$ and $[3_1 \times 4_1]^{(5)}$. At least four E6 one-phonon configurations are involved below 4 MeV and most of the 6^+ states have a dominant one-phonon component.

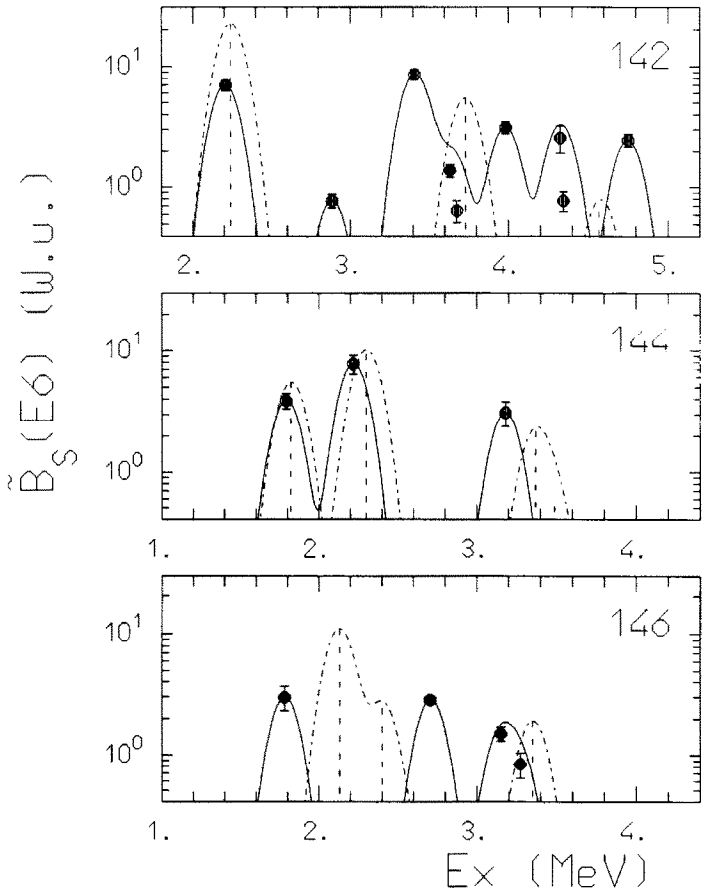

Fig. 13. Experimental E6 strengths (full points and curves) compared with QPM evaluations (dashed lines and dash-dotted curves).

6.6. ISOVECTOR COMPONENTS

As shown in eq. (5) the isovector matrix elements can be obtained from the difference between (p, p') and (d, d') matrix elements and allow an estimate of the difference $(M_n - M_p)$. Positive (negative) $\tilde{M}_V$ values indicate dominant neutron (proton) components in the transition amplitudes. Most of the states obtained from RPA calculations are due to rather pure proton (or neutron) configurations. Shell effects are clearly present in ^{142}Nd and ^{144}Nd where the main component in the low-lying states is often due to a proton two-quasi-particle configuration. QPM states have a more complex structure with a larger mixing of proton and neutron configurations. As a consequence M_V values are frequently positive and the ratio M_V/M_S, which is equal to $(M_n - M_p)/(M_n + M_p)$, is usually <1. This result is more in agreement with the collective model predictions.

To give examples of both absolute and relative values of the isovector components, the M_V(E3) matrix elements in the four nuclei, for which QPM calculations have been performed, are shown in fig. 14, while the ratios M_V(E4)/M_S(E4) are shown in fig. 15. The QPM curves have been obtained using the same effective charges adopted for the calculations shown in the figs. 6, 8, 10, 12 and 13, i.e. $e_p = 1.1e$ and $e_n = 1.3e$. This small difference between the two effective charges gives a small, but rather clear improvement in the agreement with the experimental data. This could

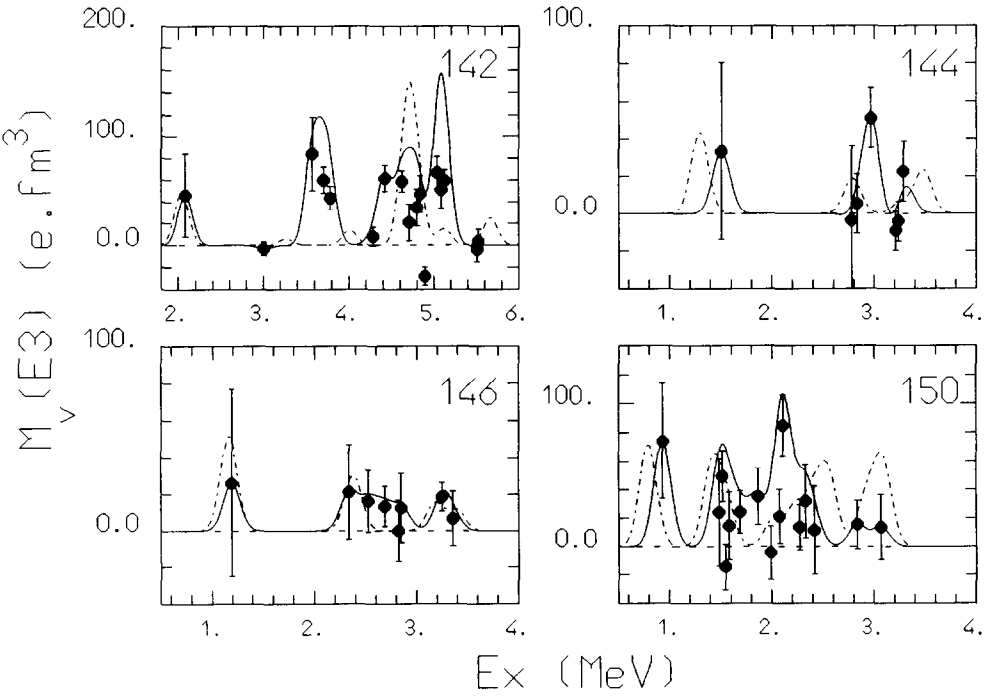

Fig. 14. Experimental E3 isovector matrix elements (full points and curves) compared with QPM evaluations (dash-dotted curves).

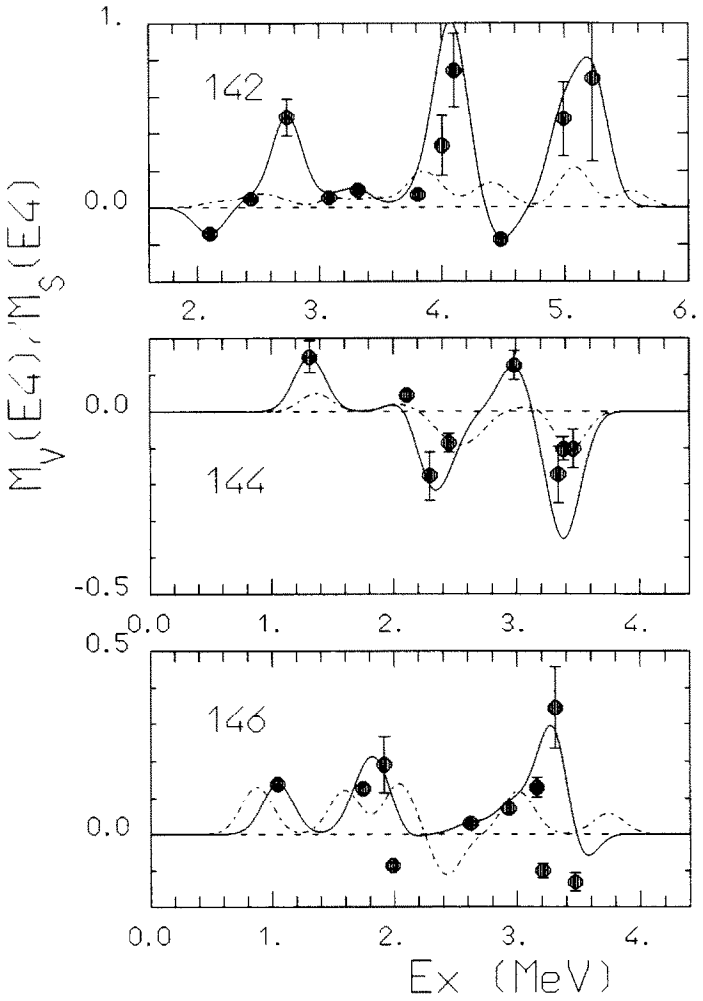

Fig. 15. Ratios of the isovector to the isoscalar E4 matrix elements in the isotopes indicated in the figures compared with QPM evaluations (dash-dotted curves).

be an indication that the limited model space is affecting more the neutron than the proton part of the wave function. With these effective charges a satisfactory overall agreement is obtained. Practically the same results for the isoscalar components are obtained assuming $e_p = e_n = 1.2e$. This is due to their much lower sensitivity to differences between the two effective charges. Finally it must be remarked that the same effective charges have been used for all the isotopes and all the multipolarities. A mass dependence of these parameters would, however, be useful to improve the agreement in a comparison limited to only the 2_1^+ and the 3_1^- states.

7. Summary and conclusions

Proton- and deuteron-scattering experiments have been performed on the stable, even-A Nd isotopes. The good energy resolution made it possible to identify many transitions of different multipolarities. Several new levels have been observed. $B(E\lambda)$ values have been determined by assuming a surface-peaked transition potential. The collected data allow systematic investigation of the modes of excitation of these low-lying states.

Special attention has been given in this respect to the interplay between the different degrees of freedom. To this end, the experimental results were compared with calculations in the framework of the interacting boson model (IBM) and of the quasi-particle–phonon model (QPM). The latter is a microscopic model in which the basis states, called "phonons", are the collective and the non-collective solutions of the BCS quasi-particle RPA equations. The fact that the QPM is taking into account not only the strong collective configurations, but also states with a weaker collectivity down to quasi-particle states is of some interest in comparing with experimental results including also weak transitions. In a second step of the QPM evaluations, two- and three-phonon states are constructed and simultaneously coupled and mixed. The interplay between the different multi-phonon configurations has an essential role in determining the gross structure of the different strength distributions. This is especially evident in the case of even-parity transitions (E2, E4 and E6), in which several one- and two-phonon configurations are of some importance. The model describes reasonably well the isoscalar and isovector strength distributions for the different multipolarities from $\lambda = 2$ to $\lambda = 6$.

Even-parity transitions are not well described by the IBM evaluations except for the transitions to the lowest states. This has been interpreted as evidence of the need of introducing higher-lying even-parity bosons. Also the fact that the collective IBM subspace is completely decoupled from the quasi-particle subspace can play a certain role in this respect. IBM-sdf evaluations are quite successful in describing the octupole strength distribution, as due to the fragmentation of the f-boson strength. This result corresponds in the QPM description to the fact that the same strength distribution is described in spherical nuclei as the fragmentation of only one E3 phonon, in contrast with the other multipolarities. IBM-sdf also gives a reasonable description of the isocalar transition strengths to the lowest dipole states.

Part of this work was performed within the research program of the Stichting voor Fundamenteel Onderzoek der Materie (FOM) with financial support of the Nederlandse Organisatie voor Wetenschappelijk Onderzoek (NWO).

References

1) L.K. Peker, Nucl. Data Sheets **59** (1990) 393; **60** (1990) 953; **63** (1991) 647;
J.K. Tuli, Nucl. Data Sheets **56** (1989) 607;
E. der Mateosan, Nucl. Data Sheets **48** (1986) 345

2) R.K.J. Sandor, H.P. Blok, U. Garg, M.N. Harakeh, C.W. de Jager, V.Yu. Ponomarev, A.I. Vdovin and H. de Vries, Phys. Lett. **B233** (1989) 54; Nucl. Phys. **A535** (1991) 669
3) R.K.J. Sandor, H.P. Blok, U. Garg, M. Girod, M.N. Harakeh, C.W. de Jager and H. de Vries, Phys. Rev. **C34** (1991) R2040 and to be published
4) R.K.J. Sandor, H.P. Blok, M. Girod, M.N. Harakeh, C.W. de Jager, V.Yu. Ponomarev and H. de Vries, Nucl. Phys. **A551** (1993) 378
5) M. Pignanelli, N. Blasi, S. Micheletti, R. De Leo, M.A. Hofstee, J.M. Schippers, S.Y. van der Werf and M.N. Harakeh, Nucl. Phys. **A519** (1990) 567
6) M. Pignanelli, N. Blasi, S. Micheletti, R. De Leo, L. Lagamba, R. Perrino, J.A. Bordewijk, M.A. Hofstee, J.M. Schippers, S.Y. van der Werf, J. Wesseling and M.N. Harakeh, Nucl. Phys. **A540** (1992) 27
7) Y. Fujita, M. Fujiwara, S. Morinobu, I. Katayama, T. Yamazaki, T. Itahashi, H. Ikegami and I.S. Hayakawa, Phys. Rev. **C40** (1989) 1595
8) V.G. Soloviev, Theory of complex nuclei (Pergamon, Oxford, 1976)
9) V.G. Soloviev, Z. Phys **A334** (1989) 143;
V.G. Soloviev and N.Yu. Shirikova, Z. Phys. **A334** (1989) 149
10) A. Arima and F. Iachello, Ann. of Phys. **111** (1978) 201
11) ECIS, coupled channel code by J. Raynal, private communication
12) F.D. Becchetti and G.W. Greenlees, Phys. Rev. **182** (1969) 1190
13) W.W. Daehnick, J.D. Childs and Z. Vrcelj, Phys. Rev. **C21** (1980) 2253
14) G.R. Satchler, J. Math. Phys. **13** (1972) 1118
15) A.M. Bernstein, V.R. Brown and V.A. Madsen, Phys. Lett. **B71** (1977) 49
16) A. Bohr and B.R. Mottelson, Nuclear structure, vol. 2 (Benjamin, New York, 1975) p. 553
17) M.N. Harakeh, KVI internal report 77 (1981)
18) J.P. Jeukenne, A. Lejeunne and C. Mahaux, Phys. Rev. **C16** (1977) 80
19) T. Tamura, Rev. Mod. Phys. **37** (1965) 679
20) D.K. Srivastava and H. Rebel, Z. Phys. **A316** (1984) 225
21) H.H. Pitz, R.D. Heil, U. Kneissl, S. Lindenstruth, U. Seemann, R. Stock, C. Wesselborg, A. Zilges, P. von Brentano, S.D. Hoblit and A.M.N. Nathan, Nucl. Phys. **A509** (1990) 587
22) O. Sholten, Ph.D. Thesis, University of Groningen, The Netherlands (1980), unpublished
23) O. Sholten, the programs PHINT and FBEM, KVI internal report 63 (1979), revised (1987), private communication
24) A.F. Barfield, B.R. Barrett, J.L. Wood and O. Scholten, Ann. of Phys. **182** (1988) 344
25) H.C. Wu, A.E.L. Dieperink, O. Scholten, M.N. Harakeh, R. De Leo, M. Pignanelli and I. Morrison, Phys. Rev. **C38** (1988) 1638
26) F.A. Gareev, S.P. Ivanova, V.G. Soloviev and S.I. Fedotov, Sov. J. Part. Nucl. **4** (1973) 357
27) R. Perrino, N. Blasi, R. De Leo, M.N. Harakeh, C.W. de Jager, S. Micheletti, M. Pignanelli, V.Yu. Ponomarev, R.J.K. Sandor and H. de Vries, to be publishedin Nucl. Phys. A
28) V.G. Soloviev and A.V. Sushkov, Phys. Lett. **B262** (1991) 29
29) A.F. Barfield, P. von Brentano, A. Dewald, K.O. Zell, N.V. Zamfir, D. Bucurescu, I. Ivascu and O. Scholten, Z. Phys. **A332** (1989) 29
30) P. von Brentano, N.V. Zamfir and A. Zilges, Phys. Lett. **B278** (1992) 221
31) D.T. Khoa, V.Yu. Pomarev and V.V. Voronov, Bull. Acad. Sci. USSR, Phys. Ser. **48** (1984) 190